

# TopoFR: A Closer Look at Topology Alignment on Face Recognition

Jun Dan<sup>\*1,2</sup>, Yang Liu<sup>\*2,3</sup>, Jiankang Deng<sup>4</sup>, Haoyu Xie<sup>2,5</sup>, Siyuan Li<sup>2</sup>,  
Baigui Sun<sup>†2,5</sup>, Shan Luo<sup>3</sup>

<sup>1</sup>Zhejiang University <sup>2</sup>FaceChain Community <sup>3</sup>King’s College London

<sup>4</sup>Imperial College London <sup>5</sup>Alibaba Group

danjun@zju.edu.cn, {yang.15.liu, shan.luo}@kcl.ac.uk, j.deng16@imperial.ac.uk  
xiehaoyu.xhy@alibaba-inc.com, sunbaigui85@gmail.com

## Abstract

The field of face recognition (FR) has undergone significant advancements with the rise of deep learning. Recently, the success of unsupervised learning and graph neural networks has demonstrated the effectiveness of data structure information. Considering that the FR task can leverage large-scale training data, which intrinsically contains significant structure information, we aim to investigate how to encode such critical structure information into the latent space. As revealed from our observations, directly aligning the structure information between the input and latent spaces inevitably suffers from an overfitting problem, leading to a structure collapse phenomenon in the latent space. To address this problem, we propose TopoFR, a novel FR model that leverages a topological structure alignment strategy called PTSA and a hard sample mining strategy named SDE. Concretely, PTSA uses persistent homology to align the topological structures of the input and latent spaces, effectively preserving the structure information and improving the generalization performance of FR model. To mitigate the impact of hard samples on the latent space structure, SDE accurately identifies hard samples by automatically computing structure damage score (SDS) for each sample, and directs the model to prioritize optimizing these samples. Experimental results on popular face benchmarks demonstrate the superiority of our TopoFR over the state-of-the-art methods. Code and models are available at: [https://github.com/modelscope/facechain/tree/main/face\\_module/TopoFR](https://github.com/modelscope/facechain/tree/main/face_module/TopoFR).

## 1 Introduction

Face recognition (FR) is a critical biometric authentication technique that is widely applied in various applications. In recent years, convolutional neural networks (CNNs) have achieved remarkable success in FR task, thanks to their powerful ability to autonomously extract face features from images. Existing studies on FR primarily focuses on constructing more discriminative face features by developing margin-based loss functions [1, 2, 3, 4, 5] and powerful network architectures [6, 7, 8, 9]. Recently, the success of unsupervised learning [10, 11, 12, 13, 14] and graph neural networks [15, 16, 17] has demonstrated the importance of data structure information in improving model generalization. However, to the best of our knowledge, how to effectively mine the potential structure information in large-scale face data has not investigated. Thus, in this paper, we extend our interests on building a cutting-edge FR framework through exploiting such powerful and substantial structure information.

First, we use Persistent Homology (PH) [20, 21], a mathematical tool used in topological data analysis [22] to capture the underlying topological structure of complex point clouds, to investigate

<sup>\*</sup> Equal Contribution, <sup>†</sup> Corresponding Author.

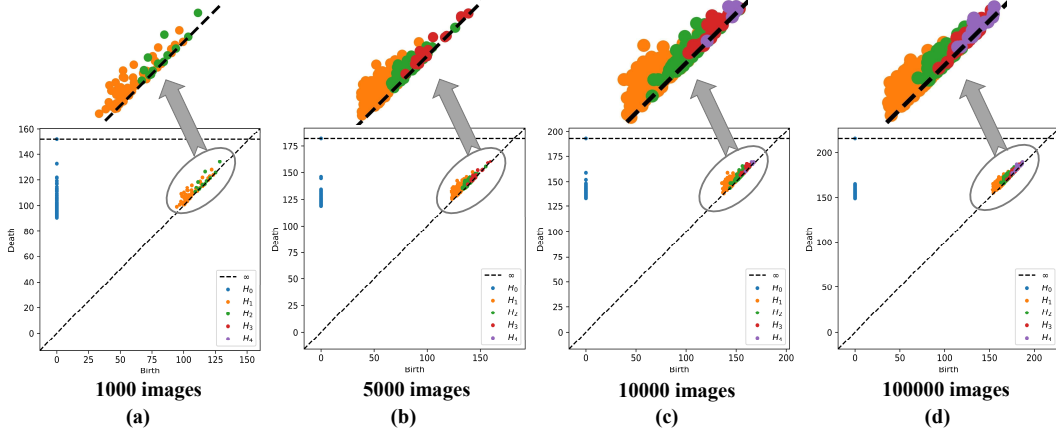


Figure 1: We sample 1000 (a), 5000 (b), 10000 (c) and 100000 (d) face images from the MS1MV2 dataset respectively, and compute their persistence diagrams using PH, where  $H_j$  represents the  $j$ -th dimension homology. Persistence diagram [18] is a mathematical tool to describe the topological structure of space, where the  $j$ -th dimension homology  $H_j$  in persistence diagram represents the  $j$ -th dimension hole in space. In topology theory, if the number of high-dimensional holes in the space is more, then the underlying topological structure of the space is more complex [19]. As shown in Figure 1(a)-1(d), as the amount of face data increases, the persistence diagram of the input space contains more and more high-dimensional holes (e.g.,  $H_3$  and  $H_4$ ). Therefore, this phenomenon demonstrates a growing complexity in the topological structure of the input space.

the evolution trend of structure information in existing FR framework and illustrate 3 interesting observations: (1) as the amount of data increases, the topological structure of the input space becomes more and more complex, as verified in Figures 1a-1d; (2) as the amount of data increases, the topological structure discrepancy between the input space and the latent space becomes increasingly larger, as verified in Figure 2a; (3) The results in Figure 2b demonstrate that as the depth of the network increases, the topological structure discrepancy becomes progressively smaller. This finding also provides an explanation for why models with more complex structure achieve higher FR accuracy. Based on the above observations, we can infer that in FR tasks with large-scale datasets, the structure of face data will be severely destroyed during training, which limits the generalization ability of FR models in practical application scenarios. To this end, we propose to improve the generalization performance of FR models by preserving the structure information.

However, we experimentally find that directly using PH to align the topological structures of the input space and the latent space may cause the model to suffer from **structure collapse phenomenon**. Concretely, under this experimental setting, we have 2 following quantitative results: (1) As shown in Figure 2c, the topological structure discrepancy drops to 0 dramatically during early training. (2) As depicted in Figure 2d, when evaluating on the IJB-C benchmark [23], there exists a significant structure information gap between the input space and the latent space. These typical overfitting phenomena indicate the latent space fails to preserve the structure information of input space accurately.

To remedy this issue, we propose a superior FR model named **TopoFR** that leverages a Perturbation-guided Topological Structure Alignment (**PTSA**) strategy to adequately preserve the topological structure information of the input space in corresponding latent face features. PTSA first employs a random structure perturbation (**RSP**) mechanism perturb the latent space and effectively increase its structure diversity. Then PTSA utilizes an invariant structure alignment (**ISA**) mechanism to align the topological structures of the original input space and the perturbed latent space, resulting in face features with stronger generalization ability

Moreover, in practical FR scenarios, the training dataset typically includes some low-quality face samples (*i.e.*, hard samples) that are prone to being encoded into abnormal positions close to the decision boundary in the latent space [24, 6, 25, 26], significantly destroying the topological structure of the latent space and affecting the alignment of structure. To address this issue, we propose a novel hard sample mining strategy named Structure Damage Estimation (**SDE**). SDE adaptively assigns structure damage score (**SDS**) to each sample based on its prediction uncertainty and prediction

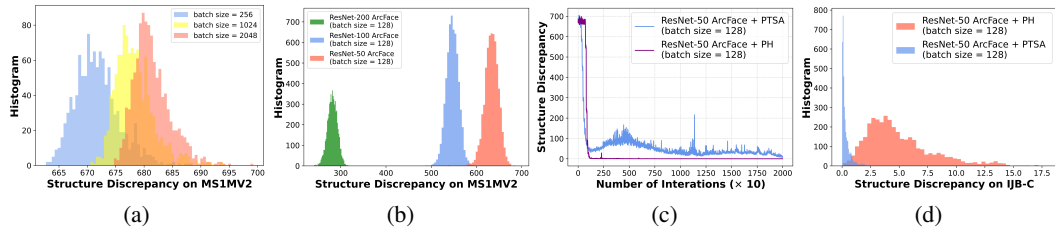


Figure 2: **(a):** We investigate the relationship between the amount of data and the topological structure discrepancy by employing ResNet-50 ArcFace model [1] to perform inferences on MS1MV2 training set. Inferences are conducted for 1000 iterations with batch sizes of 256, 1024, and 2048, respectively. Histograms are used to approximate these discrepancy distributions. **(b):** We investigate the relationship between the network depth and the topological structure discrepancy by performing inference on MS1MV2 training set (batch size=128) using ArcFace models with different backbones. **(c):** We investigate the trend of topological structure discrepancy during training (batch size=128) and found that **i**) directly using PH to align the topological structures will cause the discrepancy to drop to 0 dramatically; **ii**) whereas using our PTSA strategy promotes a smooth convergence of structure discrepancy. **(d):** Aligning the topological structures directly using PH will lead to significant discrepancy when evaluating on IJB-C benchmark. Our PTSA strategy effectively mitigates this overfitting issue, resulting in smaller structure discrepancy during evaluation.

probability. By prioritizing the optimization of hard samples with significant structure damage, SDE can gradually guide these samples back to their reasonable positions, thereby improving the generalization ability of FR model.

In summary, the main contributions are listed as follows:

- 1) To the best of knowledge, we are the first to explore the topological structure alignment in FR task. We propose a novel topological structure alignment strategy called PTSA to effectively align the structures of the original input space and the perturbed latent space.
- 2) A novel hard sample mining strategy named SDE is introduced to mitigate the adverse impact of hard samples on the latent space structure.
- 3) Experimental results show that the proposed method outperforms SOTA methods on various face benchmarks. Notably, our TopoFR has secured **the second place** in the ICCV21 MFR-Ongoing challenge [27] until the submission of this work (May 22 '24, academic track): <http://iccv21-mfr.com/#/leaderboard/academic>, indicating the robustness and generalization of our method.

## 2 Related Works

**Face Recognition (FR).** Convolutional Neural Networks (CNNs) [28, 29] have achieved remarkable advancements in tasks related to facial recognition [30, 31, 32, 1, 33, 34]. Notably, the extraction of robust deep facial embeddings has raised considerable interest within the research community. Among them, CNNs framework are representative methods, using two primary methods: metric learning-based and margin-based softmax approaches. The former utilizes loss functions like Triplet loss [7], Tuplet loss [35], and Center loss [36] to learn discriminative face features, while the latter aims to incorporate margin penalty into the softmax loss framework, including methods such as ArcFace [1], CosFace [2], AM-softmax [37], and SphereFace [38]. Recent studies have explored various techniques, including adaptive parameters [3, 5], mining [4, 39, 40], learning acceleration [41, 42, 43], vision transformer architecture [9, 8], and data uncertainty [25, 6, 26] to further enhance models' performance on large-scale datasets.

**Persistent Homology (PH).** Over the past decade, PH has shown significant advantages in multiple various such as signal processing[44], video analysis [45, 46], neuroscience [47, 48], disease diagnosis [49] and evaluation of embedding strategies [50, 51]. In the field of machine learning, some studies [52, 53, 54] have shown that integrating topological representations into network can enhance model's recognition/segmentation performance. [55] proposes a topology distance for the evaluation of GANs.

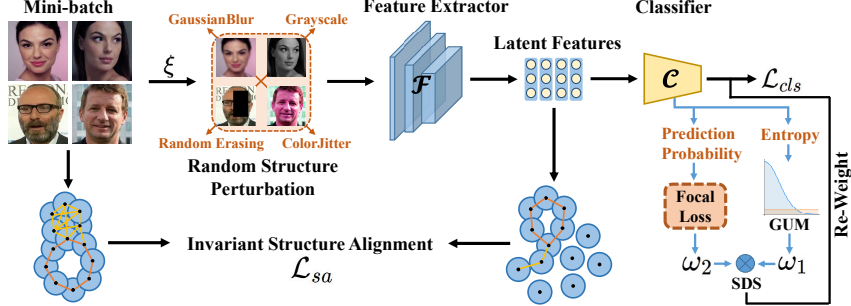


Figure 3: Global overview of our proposed TopoFR.  $\otimes$  represents the multiplication operation.  $\xi$  denotes the probability of applying RSP to each training sample.

### 3 Background: Persistent Homology

PH is a computational topology method that quantifies the changes in the topological invariants of a Vietoris-Rips complex as a scale parameter  $\rho$  is varied. In this section, we introduce some key concepts of PH. Further details on PH can be found in Refs. [20, 56].

**Notation.**  $\mathcal{X} := \{x_i\}_{i=1}^n$  represents a point cloud and  $\mu : \mathcal{X} \times \mathcal{X} \rightarrow \mathbb{R}$  denotes a distance metric over  $\mathcal{X}$ . Matrix  $\mathcal{M}$  represents the pairwise distances (*i.e.*, Euclidean distance) between points in  $\mathcal{X}$ .

**Vietoris-Rips Complex.** The Vietoris-Rips complex [57] is a special simplicial complex constructed from a set of points in a metric space, and it can be used to approximate the topology of the underlying space. For  $0 \leq \rho < \infty$ , we represent the Vietoris-Rips complex of point cloud  $\mathcal{X}$  at scale  $\rho$  as  $\mathcal{V}_\rho(\mathcal{X})$ , which contains all simplices (*i.e.*, subsets) of  $\mathcal{X}$ , and each component of point cloud  $\mathcal{X}$  satisfies a distance constraint:  $\mu(x_i, x_j) \leq \rho$  for any  $i, j$ . Moreover, the Vietoris-Rips complex satisfies a nesting relation, *i.e.*,  $\mathcal{V}_{\rho_i} \subseteq \mathcal{V}_{\rho_j}$  for any  $\rho_i \leq \rho_j$ , which allows us to track the evolution progress of simplicial complex as the scale  $\rho$  increases. It is worth noting that  $\mathcal{V}_\rho(\mathcal{X})$  and  $\mathcal{V}_\rho(\mathcal{M})$  are equivalent because constructing the Vietoris-Rips complex only requires distance.

**Homology Group.** The homology group [58] is an algebraic structures that analyzes the topological features of a simplicial complex in different dimension  $j$ , such as connected components ( $H_0$ ), cycles ( $H_1$ ), voids ( $H_2$ ), and higher-dimensional features ( $H_j$ ,  $j \geq 3$ ). By tracking the changes in topological features ( $H_j$ ) of the Vietoris-Rips complex as the scale  $\rho$  increases, it is possible to gain insight into the multi-scale topological information of the underlying space.

**Persistence Diagram and Persistence Pairing** [59]. The persistence diagram  $\mathcal{D}$  is a multi-set of points  $(b, d)$  in the Cartesian plane  $\mathbb{R}^2$ , which encodes information about the lifespan of topological features. Specially, it summarizes the birth time  $b$  and death time  $d$  of each topological feature, where birth time  $b$  signifies the scale at which the feature is created and death time  $d$  refers to the scale at which it is destroyed. The persistence pairing  $\gamma$  contains indices  $(i, j)$  corresponding to simplices  $r_i, r_j \in \mathcal{V}_\rho(\mathcal{X})$  that create and destroy the topological features identified by  $(b, d) \in \mathcal{D}$ , respectively.

### 4 Methodology

In this paper, we propose a novel framework named **TopoFR** for constraining the FR model to preserve the topological structure information of the input space in their latent features. The architecture of our TopoFR model is depicted in Figure 3. It consists of two components: a feature extractor  $\mathcal{F}$  and an image classifier  $\mathcal{C}$ . Mathematically, given an input image  $x$ , the latent feature extracted by  $\mathcal{F}$  is denoted as  $f = \mathcal{F}(x) \in \mathbb{R}^l$ , and the classification probability predicted by  $\mathcal{C}$  is denoted as  $g = \mathcal{C}(f) \in \mathbb{R}^K$ , where  $l$  represents the feature dimension and  $K$  denotes the number of classes. The entropy of the classification prediction probability  $g$  can be represented as  $E(g) = -\sum_{k=1}^K g^k \log g^k$ , where  $g^k$  is the probability of predicting a sample to class  $k$ .

## 4.1 Perturbation-guided Topological Structure Alignment

As mentioned in Section 1, directly applying PH to align the topological structures of the input space and the latent space can cause the FR model to encounter structure collapse phenomenon. To remedy this problem, we propose a Perturbation-guided Topological Structure Alignment (**PTSA**) strategy that includes two mechanisms: random structure perturbation and invariant structure alignment.

**Random Structure Perturbation (RSP).** PTSA first utilizes the RSP mechanism to randomly perturb the structure of the latent space. Specially, it utilizes a data augmentation list  $\mathcal{A} = \{\mathcal{A}_1, \mathcal{A}_2, \mathcal{A}_3, \mathcal{A}_4\}$  that includes four common data augmentation operations, namely Random Erasing  $\mathcal{A}_1$ , GaussianBlur  $\mathcal{A}_2$ , Grayscale  $\mathcal{A}_3$  and ColorJitter  $\mathcal{A}_4$ . For each training sample  $x_i$ , RSP will randomly select an operation  $\mathcal{A}_r$  from  $\mathcal{A}$  to perturb it, *i.e.*,  $\tilde{x}_i = \mathcal{A}_r(x_i)$ . Then the perturbed sample  $\tilde{x}_i$  will be fed into the model for supervised learning, which effectively increases the structure diversity of the latent space. In our model, we adopt ArcFace loss [1] as the basic classification loss:

$$\mathcal{L}_{arc}(\tilde{x}_i, y_i) = -\log \frac{e^{s(\cos(\theta_i^y + m))}}{e^{s(\cos(\theta_i^y + m))} + \sum_{k=1, k \neq y}^K e^{s \cos \theta_i^k}}, \quad (1)$$

where  $y_i$  is the class label of the original image  $x_i$ ,  $s$  is a scaling parameter,  $\theta_i^k$  is the angle between the  $k$ -th class center and feature, and  $m$  denotes an additive angular margin. During training, we apply the RSP mechanism to each sample  $x_i$  with a probability  $\xi$  of 0.2.

**Invariant Structure Alignment (ISA).** Given a mini-batch of original training samples  $\mathcal{X} = \{x_i\}_{i=1}^n$ , we denote the perturbed batch samples as  $\tilde{\mathcal{X}} = \{\tilde{x}_i\}_{i=1}^n$ . For the perturbed samples, we denote the latent features extracted by  $\mathcal{F}$  as  $\tilde{\mathcal{Z}} = \{\tilde{f}_i\}_{i=1}^n$ . During forward propagation, we can construct the Vietoris-Rips complexes  $\mathcal{V}_\rho(\mathcal{X})$  and  $\mathcal{V}_\rho(\tilde{\mathcal{Z}})$  for point clouds  $\mathcal{X}$  and  $\tilde{\mathcal{Z}}$  respectively, based on their respective pairwise distance matrix  $\mathcal{M}^{\mathcal{X}}$  and  $\mathcal{M}^{\tilde{\mathcal{Z}}}$ . Then we can utilize persistent homology to analyze the topological structures of  $\mathcal{V}_\rho(\mathcal{X})$  and  $\mathcal{V}_\rho(\tilde{\mathcal{Z}})$ , and obtain their corresponding persistence diagrams  $\{\mathcal{D}^{\mathcal{X}}, \mathcal{D}^{\tilde{\mathcal{Z}}}\}$  and persistence pairings  $\{\gamma^{\mathcal{X}}, \gamma^{\tilde{\mathcal{Z}}}\}$ , respectively.

Ideally, no matter how the face image is perturbed, the position of the encoded face feature in the latent space should remain unchanged, and the topological structure of the perturbed latent space should also be consistent with the original input space. To this end, we choose to align the original input space  $\mathcal{X}$  with the perturbed latent space  $\tilde{\mathcal{Z}}$  to achieve this goal. Prior studies usually utilize bottleneck distance or Wasserstein distance to measure the topological structure discrepancy [60, 18] between two spaces by comparing the differences in persistence diagrams. However, these two metrics are sensitive to outliers in persistence diagrams [55, 61] and will significantly increase models' training time, rendering them unsuitable for FR tasks with extremely large-scale datasets, as verified in Table 8 in the Appendix.

To mitigate this issue, we turn to retrieve the persistence diagrams values by subsetting the corresponding pairwise distance matrix with edge indices provided by the persistence pairings [62, 63, 64], *i.e.*,  $\mathcal{D}^{\mathcal{X}} \simeq \mathcal{M}^{\mathcal{X}}[\gamma^{\mathcal{X}}]$  and  $\mathcal{D}^{\tilde{\mathcal{Z}}} \simeq \mathcal{M}^{\tilde{\mathcal{Z}}}[\gamma^{\tilde{\mathcal{Z}}}]$ . By comparing the difference between two topologically relevant distance matrices from both spaces, we can quickly and stably compute the discrepancy between their persistence diagrams, providing an efficient solution for structure alignment of FR models driven by large-scale datasets. We formulate the ISA loss as follows:

$$\mathcal{L}_{sa}(\mathcal{D}^{\mathcal{X}}, \mathcal{D}^{\tilde{\mathcal{Z}}}) = \frac{1}{2} \left( \left\| \mathcal{M}^{\mathcal{X}}[\gamma^{\mathcal{X}}] - \mathcal{M}^{\tilde{\mathcal{Z}}}[\gamma^{\mathcal{X}}] \right\|^2 + \left\| \mathcal{M}^{\tilde{\mathcal{Z}}}[\gamma^{\tilde{\mathcal{Z}}}] - \mathcal{M}^{\mathcal{X}}[\gamma^{\tilde{\mathcal{Z}}}] \right\|^2 \right) \quad (2)$$

**Notably**, in the field of FR, most existing works do not include any data augmentation operations, as this would introduce more unidentifiable face images (*i.e.*, destroying the fidelity of each face), which generally hurts the FR model's generalization ability, as verified in Refs. [3, 65]. In this work, we do not employ these data augmentations to simply augment data scale. Instead, we use them to increase the latent space's structure diversity, effectively addressing the structure collapse problem. As a result, our PTSA strategy can reap the benefits of data augmentations while mitigating their potential negative effects (see Figure 2, Table 3, and Figure 5 for further analysis.).

## 4.2 Structure Damage Estimation

In practical FR scenarios, low-quality face samples, also known as "hard samples", are commonly included in the training set. These hard samples tend to be encoded in abnormal positions near the decision boundary in the latent space [25, 6, 66, 67], which will disrupt the latent space's topological structure and further hinder the alignment of structures. To address this issue, we propose a novel hard sample mining strategy called Structure Damage Estimation (**SDE**). SDE is specifically designed to identify hard samples with serious structure damage within the training set accurately. By prioritizing the learning of these hard samples and guiding them back to the reasonable positions during optimization, SDE aims to mitigate the adverse impact of hard samples on the latent space's topological structure.

**Prediction Uncertainty.** Hard samples are typically distributed near the decision boundary, thus have a high prediction uncertainty (*i.e.*, large entropy of the classifier prediction) and are more likely to be misclassified by the classifier [68, 69, 70, 71]. Conversely, easy samples are usually located far from the decision boundary and have relatively low prediction uncertainty. To model the difficulty of each sample, we introduce a binary random variable  $u_i \in \{0, 1\}$  for each sample  $\tilde{x}_i$  to indicate whether the sample is hard or easy by values of 1 and 0, respectively. Then the probability that sample  $\tilde{x}_i$  belongs to hard samples (*i.e.*, with large prediction uncertainty) can be defined as  $h_\varphi(\tilde{x}_i) = P_\varphi(u_i = 1|\tilde{x}_i)$ , where  $\varphi$  represents the parameter set. According to the cluster assumption [72, 73], we believe that samples with higher prediction entropy are more disruptive to the latent space's topological structure. Therefore, we propose to model the distribution of the entropy  $E(\tilde{g}_i)$  for each training sample  $\tilde{x}_i$  using the Gaussian-uniform mixture (**GUM**) model, a statistical distribution that is robust to outliers [74, 75, 76]:

$$p(E(\tilde{g}_i)|\tilde{x}_i) = \pi\mathcal{N}^+(E(\tilde{g}_i)|0, \Sigma) + (1 - \pi)\mathcal{U}(0, \Omega), \quad (3)$$

where

$$\mathcal{N}^+(a|0, \Sigma) = \begin{cases} 2\mathcal{N}(a|0, \Sigma), & a \geq 0, \\ 0, & a < 0. \end{cases} \quad (4)$$

$\mathcal{U}(0, \Omega)$  is a uniform distribution defined on  $[0, \Omega]$ ,  $\pi$  is a prior probability, and  $\Sigma$  is the variance of Gaussian distribution  $\mathcal{N}(a|0, \Sigma)$ . In this mixed model, the uniform distribution term  $\mathcal{U}$  and the Gaussian distribution term  $\mathcal{N}^+$  respectively model the hard samples and easy samples. Then the posterior probability that the sample  $\tilde{x}_i$  to be hard (*i.e.*, high-uncertainty) can be computed as follows:

$$h_\varphi(\tilde{x}_i) = P_\varphi(u_i = 1|\tilde{x}_i) = \frac{(1 - \pi)\mathcal{U}(0, \Omega)}{\pi\mathcal{N}^+(E(\tilde{g}_i)|0, \Sigma) + (1 - \pi)\mathcal{U}(0, \Omega)}. \quad (5)$$

In Equation (5), when the classifier prediction is close to uniform distribution or when the prediction probabilities for multiple classes are nearly equal, the posterior probability of a sample belonging to hard data will be very high, *i.e.*,  $(\tilde{g}_i \rightarrow [\frac{1}{K}, \frac{1}{K}, \dots, \frac{1}{K}], h_\varphi(\tilde{x}_i) \rightarrow 1)$ , otherwise it is relatively low. Hence, the prediction uncertainty of sample  $\tilde{x}_i$  can be measured by a quantitative probability  $h_\varphi(\tilde{x}_i)$ .

Assume  $\hat{E}(\tilde{g}_i) = (-1)^{\epsilon_i} E(\tilde{g}_i)$ ,  $\epsilon_i \sim B(1, 0.5)$ , where  $B$  is a Bernoulli distribution [77], then the variable  $\hat{E}(\tilde{g}_i)$  obeys the following statistical distribution:

$$p(\hat{E}(\tilde{g}_i)|\tilde{x}_i) = \pi\mathcal{N}(\hat{E}(\tilde{g}_i)|0, \Sigma) + (1 - \pi)\mathcal{U}(-\Omega, \Omega). \quad (6)$$

In this way, the maximum likelihood model of Equation (6) can be formulated as:  $\max_{\pi, \Sigma, \Omega} \prod_{i=1}^n p(\hat{E}(\tilde{g}_i)|\tilde{x}_i)$ . Then, the parameter set  $\varphi = \{\pi, \Sigma, \Omega\}$  of GUM can be estimated via the Expectation-Maximization (EM) algorithm [78] with the following iterative formulas:

$$\begin{aligned} h_\varphi^{(t+1)}(\tilde{x}_i) &= \frac{(1 - \pi^{(t)})\mathcal{U}(-\Omega^{(t)}, \Omega^{(t)})}{\pi^{(t)}\mathcal{N}(\hat{E}(\tilde{g}_i)|0, \Sigma^{(t)}) + (1 - \pi^{(t)})\mathcal{U}(-\Omega^{(t)}, \Omega^{(t)})}, \quad \pi^{(t+1)} = \frac{\sum_{i=1}^n (1 - h_\varphi^{(t+1)}(\tilde{x}_i))}{n}, \\ \Sigma^{(t+1)} &= \frac{\sum_{i=1}^n (1 - h_\varphi^{(t+1)}(\tilde{x}_i))(\hat{E}(\tilde{g}_i))^2}{\sum_{i=1}^n (1 - h_\varphi^{(t+1)}(\tilde{x}_i))}, \quad \Omega^{(t+1)} = \sqrt{3(\eta_2 - \eta_1^2)}, \end{aligned} \quad (7)$$

where

$$\eta_1 = \frac{\sum_{i=1}^n \frac{h_\varphi^{(t+1)}(\tilde{x}_i)}{1-\pi^{(t+1)}} \hat{E}(\tilde{g}_i)}{\sum_{i=1}^n (1 - h_\varphi^{(t+1)}(\tilde{x}_i))}, \eta_2 = \frac{\sum_{i=1}^n \frac{h_\varphi^{(t+1)}(\tilde{x}_i)}{1-\pi^{(t+1)}} (\hat{E}(\tilde{g}_i))^2}{\sum_{i=1}^n (1 - h_\varphi^{(t+1)}(\tilde{x}_i))}.$$

Specifically, at each iteration, EM alternates between evaluating the expected log-likelihood (E-step) and updating the parameter set  $\varphi$  (M-step). In Equation (7), the **E-step** aims to evaluate the posterior probability  $h_\varphi^{(t+1)}$  of a sample  $\tilde{x}_i$  to be hard sample using the iterative formula  $h_\varphi^{(t+1)}(\tilde{x}_i)$ , where  $(t+1)$  denotes the EM iteration index. The **M-step** updates the parameter set  $\varphi$  using the iterative formulas  $\pi^{(t+1)}$ ,  $\Sigma^{(t+1)}$  and  $\Omega^{(t+1)}$ .

**Structure Damage Score (SDS).** Compared to correctly classified samples, misclassified samples usually have larger difficulty and have greater destructive effects on the latent space's topological structure. Therefore, misclassified samples need to receive more attention during training. Inspired by the Focal loss [79], we design a probability-aware scoring mechanism  $\omega(\tilde{x}_i)$  that combines prediction uncertainty  $h_\varphi(\cdot)$  and prediction accuracy to adaptively compute SDS for each sample  $\tilde{x}_i$ :

$$\omega(\tilde{x}_i) = \omega_1(\tilde{x}_i) \times \omega_2(\tilde{x}_i) = (1 + h_\varphi(\tilde{x}_i))^\lambda \times (1 - \tilde{g}_i^{gt}), \quad (8)$$

where  $\lambda$  is a temperature coefficient, and  $\tilde{g}_i^{gt}$  represents the prediction probability of ground truth. Specifically, SDS assigns higher SDS to hard samples and lower SDS to easy samples, which effectively balances the contribution of each sample to the objective. By assigning higher scores to hard samples, the model is encouraged to focus more on learning these challenging samples, boosting the FR system's generalization. Formally, the SDS weighted classification loss  $\mathcal{L}_{cls}$  is defined as:

$$\mathcal{L}_{cls} = \omega(\tilde{x}_i) \times \mathcal{L}_{arc}(\tilde{x}_i, y_i) \quad (9)$$

During training, to minimize the objective  $\mathcal{L}_{cls}$ , the model needs to optimize both the SDS  $\omega$  and the loss  $\mathcal{L}_{arc}$ , which brings two benefits: (1) Minimizing  $\mathcal{L}_{arc}$  can encourage the model to capture face features with greater generalization ability from diverse training samples. (2) Minimizing SDS  $\omega$  can alleviate the damage of hard samples to the latent space's topological structure, which is beneficial to the preservation of topological structure information and the construction of clear decision boundary.

### 4.3 Model Optimization

To summarize, the overall objective of TopoFR can be formulated as follows:

$$\min_{\mathcal{F}, \mathcal{C}} \mathcal{L}_{cls} + \alpha \mathcal{L}_{sa} \quad (10)$$

where  $\alpha$  is hyper-parameter that balances the contributions of the loss  $\mathcal{L}_{cls}$  and the loss  $\mathcal{L}_{sa}$ . Detailed parameter sensitivity analysis can be found in Figure 6 in the Appendix.

## 5 Experiments

### 5.1 Datasets.

**i) For training**, we employ three distinct datasets, namely MS1MV2 [1] (5.8M facial images, 85K identities), Glint360K [41] (17.1M facial images, 360K identities), and WebFace42M [80] dataset (42.5M facial images, 2M identities). **ii) For evaluation**, we adopt LFW [81], AgeDB-30 [82], CFP-FP [83], CPLFW [84], CALFW [85], IJB-C [23], IJB-B [86] and the ICCV-2021 Masked Face Recognition Challenge (**MFR-Ongoing**) [27] as the benchmarks to test the performance of our models.

Notably, the MFR-Ongoing [27] is the most authoritative and comprehensive competition for evaluating FR models' generalization performance. It contains not only the existing popular test sets, such as IJB-C, but also its own MFR benchmarks, such as Mask, Children, and Multi-Racial test sets. Due to page size limitation, more training settings and experimental results are placed on **Appendix**.

### 5.2 Results on Mainstream Benchmarks

**Results on MFR-Ongoing.** We employ WebFace42M as training set, and compare our TopoFR with SOTA competitors on MFR-Ongoing challenge, as reported in Table 1. For a fair comparison, all

Table 1: Verification accuracy (%) on the MFR-Ongoing benchmark.

Method	Training Data	Venue	MFR						IJB-C		
			Mask	Children	African	Caucasian	South Asian	East Asian	MR-All	1e-5	1e-4
R200, Partial FC [43]	WebFace42M	CVPR22	91.87	-	97.79	98.70	98.54	89.52	97.70	96.93	97.97
R200, UniFace [87]		ICCV23	92.43	93.11	<b>98.14</b>	<b>98.98</b>	98.84	90.01	97.92	96.68	97.91
<b>R200, TopoFR</b>		NeurIPS24	<b>93.96</b>	<b>93.57</b>	97.97	98.71	<b>98.98</b>	<b>92.85</b>	<b>98.13</b>	<b>97.10</b>	<b>98.01</b>

Table 2: Verification accuracy (%) on LFW, CFP-FP, AgeDB-30, IJB-C and IJB-B benchmarks.

Training Data	Method	Venue	LFW	CFP-FP	AgeDB-30	IJB-C		IJB-B
						1e-5	1e-4	
MS1MV2	R50, ArcFace [1]	CVPR19	99.68	97.11	97.53	88.36	92.52	91.66
	R50, MagFace [5]	CVPR21	99.74	97.47	97.70	88.95	93.34	91.47
	R50, AdaFace [3]	CVPR22	99.82	97.86	97.85	-	96.27	94.42
	R50, <b>TopoFR</b> <sup>†</sup>	NeurIPS24	<b>99.83</b>	<b>98.24</b>	98.23	<b>94.79</b>	96.42	95.13
	R50, <b>TopoFR</b>	NeurIPS24	<b>99.83</b>	<b>98.24</b>	<b>98.25</b>	94.71	<b>96.49</b>	<b>95.14</b>
	R100, CosFace [2]	CVPR18	99.78	98.26	98.17	92.68	95.56	94.01
	R100, ArcFace [1]	CVPR19	99.77	98.27	98.15	92.69	95.74	94.09
	R100, MV-Softmax [88]	AAAI20	99.80	98.28	97.95	-	95.20	93.60
	R100, URL [65]	CVPR20	99.78	98.64	-	95.00	96.60	-
	R100, BroadFace [89]	ECCV20	<b>99.85</b>	98.63	98.38	94.59	96.38	94.97
	R100, CurricularFace [4]	CVPR20	99.80	98.37	98.32	-	96.10	94.80
	R100, MagFace+ [5]	CVPR21	99.83	98.46	98.17	94.08	95.97	94.51
	R100, SCF-ArcFace [25]	CVPR21	99.82	98.40	98.30	94.04	96.09	94.74
	R100, DAM-CurricularFace [90]	ICCV21	-	-	-	-	96.20	95.12
	R100, ElasticFace-Cos+ [91]	CVPR22	99.80	98.73	98.28	-	96.65	95.43
	R100, AdaFace [3]	CVPR22	99.82	98.49	98.05	-	96.89	95.67
	TransFace-B [9]	ICCV23	99.82	98.39	98.27	94.15	96.55	-
	R100, <b>TopoFR</b> <sup>†</sup>	NeurIPS24	<b>99.85</b>	<b>98.83</b>	<b>98.42</b>	<b>95.28</b>	<b>96.96</b>	<b>95.70</b>
	R100, <b>TopoFR</b>	NeurIPS24	<b>99.85</b>	98.71	<b>98.42</b>	95.23	96.95	<b>95.70</b>
	R200, ArcFace [1]	CVPR19	99.79	98.44	98.19	94.67	96.53	95.18
	R200, AdaFace [3]	CVPR22	99.83	98.76	98.28	94.88	96.93	95.71
	TransFace-L [9]	ICCV23	99.83	98.65	98.23	94.55	96.59	-
	R200, <b>TopoFR</b> <sup>†</sup>	NeurIPS24	<b>99.85</b>	<b>99.09</b>	<b>98.54</b>	<b>95.19</b>	<b>97.12</b>	95.77
	R200, <b>TopoFR</b>	NeurIPS24	<b>99.85</b>	99.05	98.52	95.15	97.08	<b>95.82</b>
Glint360K	R50, ArcFace [1]	CVPR19	99.78	98.77	98.28	95.29	96.81	95.30
	R50, AdaFace [3]	CVPR22	99.82	99.07	98.34	95.58	96.90	95.66
	R50, <b>TopoFR</b>	NeurIPS24	<b>99.85</b>	<b>99.28</b>	<b>98.47</b>	<b>95.99</b>	<b>97.27</b>	<b>95.96</b>
	R100, ArcFace [1]	CVPR19	99.81	99.04	98.31	95.38	96.89	95.69
	R100, AdaFace [3]	CVPR22	99.82	99.20	98.58	96.24	97.19	95.87
	TransFace-B [9]	ICCV23	99.85	99.17	98.53	96.18	97.45	-
	R100, <b>TopoFR</b>	NeurIPS24	<b>99.85</b>	<b>99.43</b>	<b>98.72</b>	<b>96.57</b>	<b>97.60</b>	<b>96.34</b>
	R200, ArcFace [1]	CVPR19	99.82	99.14	98.49	95.71	97.20	95.89
	R200, AdaFace [3]	CVPR22	99.83	99.24	98.61	95.96	97.33	96.12
	TransFace-L [9]	ICCV23	99.85	99.32	98.62	96.29	97.61	-
	R200, <b>TopoFR</b>	NeurIPS24	<b>99.87</b>	<b>99.45</b>	<b>98.82</b>	<b>96.71</b>	<b>97.84</b>	<b>96.56</b>

compared models adopt ResNet-200 as the backbone. Specially, our TopoFR surpasses the SOTA competitors UniFace and Partial FC in multiple metrics, implying the superiority of our method. Until the submission of this work (May 22 '24), the proposed TopoFR **ranks second place** on the academic track of the MFR-Ongoing leaderboard: <http://iccv21-mfr.com/#/leaderboard/academic>.

**Results on LFW, CFP-FP and AgeDB-30.** We adopt MS1MV2 and Glint360K to train our models, respectively. The results are reported in Table 2. To showcase the universality of our method, we also provide detailed experimental results of **TopoFR**<sup>†</sup> model trained by CosFace [2]. As stated in Refs.[3, 5], the performances of existing FR models on these three benchmarks have reached saturation. **1)** On MS1MV2 training set, we note that our TopoFR and TopoFR<sup>†</sup> models still obtain accuracy improvement and outperform SOTA competitors (*e.g.*, AdaFace [3] and TransFace [9]). **2)** On Glint360K training set, our TopoFR become SOTA models and surpass AdaFace and TransFace.

**Results on IJB-C and IJB-B.** We train our TopoFR on MS1MV2 and Glint360K respectively, and compare with SOTA methods on IJB-C and IJB-B benchmarks, as reported in Table 2. **1)** On MS1MV2 training set, our models obtain the best results under different backbones. For instance, our R50 TopoFR and R50 TopoFR<sup>†</sup> models greatly surpass SOTA method AdaFace and even beat most R100-based competitors. **2)** On Glint360K training set, all our models significantly outperform the cutting-edge competitor AdaFace and achieve SOTA performance. More importantly, our TopoFR even works better than ViT-based SOTA method TransFace, implying the superiority of our method.

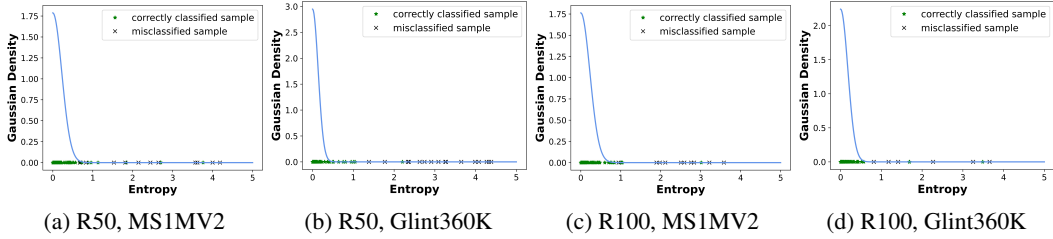


Figure 4: The estimated Gaussian density (blue curve) w.r.t the entropy of classification prediction. Green marker  $\star$  and black marker  $\times$  represent the entropy of correctly classified sample and misclassified sample, respectively.

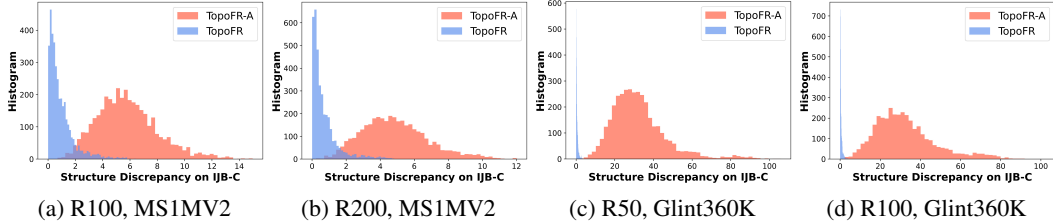


Figure 5: The topological structure discrepancy of TopoFR and variant TopoFR-A under different backbones and training datasets (*i.e.*, [Backbone, Training dataset]). Variant TopoFR-A directly utilizes PH to align the topological structures of two spaces. Notably, our TopoFR models trained with Glint360K dataset almost perfectly align the topological structures of the input space and the latent space on the IJB-C benchmark (*i.e.*, the blue histogram almost converges to a straight line).

### 5.3 Analysis and Ablation Study

Due to the limitation of page size, more ablation experiments and analysis are placed on **Appendix**.

**1) Contribution of Each Component:** To investigate the contribution of each component in our model, we employ MS1MV2 as the training set, and compare ArcFace (baseline), and four variants of TopoFR on the IJB-C benchmark. The variants of TopoFR are as follows: (1) **TopoFR-R**, the variant only adds RSP mechanism to ArcFace. (2) **TopoFR-A**, based on ArcFace, the variant simply aligns the structure of input space and latent space without using RSP. (3) **TopoFR-P**, the variant fully introduces the PTSAs strategy into ArcFace. (4) **TopoFR-G**, based on TopoFR-P, the variant only uses prediction uncertainty  $\omega_1$  modeled by GUM to re-weight each sample. (5) **TopoFR-F**, based on TopoFR-P, the variant simply applies Focal loss  $\omega_2$  to re-weight each sample.

The results gathered in Table 3 reflect some observations: (1) Compared with ArcFace, the accuracy of TopoFR-R is clearly reduced due to the addition of more unidentifiable face images, which hurts the FR model’s generalization ability. (2) TopoFR-A outperforms ArcFace, indicating that directly aligning the two spaces can slightly boost model’s performance, but it inevitably encounters structure collapse issue. (3) TopoFR-P greatly surpasses TopoFR-R and TopoFR-A, implying that preserving the structure information can greatly improve FR model’s generalization. (4) TopoFR outperforms TopoFR-F and TopoFR-G, which not only demonstrates the effectiveness of SDE strategy, but also indicates that the prediction uncertainty  $\omega_1$  is complementary to Focal loss  $\omega_2$  in mining hard samples.

**2) Effectiveness of GUM:** To visually demonstrate the effectiveness of GUM in mining hard samples, we present the estimated Gaussian density of the prediction entropy during training in Figure 4. These curves show that the entropy of misclassified face samples (represented by black crosses) usually have rather low Gaussian density (*i.e.*, high posterior probability  $h_\varphi$ ), thus can be easily detected.

Table 3: Ablation study.

Training Data	Method	IJB-C(1e-4)
MS1MV2	R50, ArcFace	92.52
	R50, TopoFR-R	92.44
	R50, TopoFR-A	93.26
	R50, TopoFR-P	95.34
	R50, TopoFR-F	95.40
	R50, TopoFR-G	96.23
	TopoFR	<b>96.49</b>

Note that even if some misclassified samples have small entropy (*i.e.*, high Gaussian density and low posterior probability  $h_\varphi$ ), their SDS  $\omega$  can still be corrected by the Focal loss  $\omega_2$ .

**3) Generalization of PTSA:** To show the superior generalization ability of our PTSA strategy in preserving structure information, we investigate the topological structure discrepancy between the input and the latent spaces of TopoFR and its variant TopoFR-A on IJB-C benchmark. Note that TopoFR-A directly utilizes PH to align the topological structures of two spaces. The results in Figure 5 indicate that: 1) Directly using PH to align the topological structures of two spaces does not effectively reduce the structure discrepancy, as the model encounters the structure collapse issue; 2) PTSA strategy can effectively align the topological structures of two spaces and address this structure collapse issue. Remarkably, Figures 5c and 5d show that our TopoFR models trained on Glint360K almost perfectly preserve structure information of input spaces in their latent features, thereby verifying the generalization of PTSA strategy.

## 6 Conclusion

This paper proposes a novel FR framework called TopoFR that aims to encode the critical structure information in large-scale face dataset into the latent space. Specially, TopoFR leverages a structure alignment strategy PTSA and a hard sample mining strategy SDE. PTSA employs PH to reduce the topological structure discrepancy between the input and latent spaces, effectively mitigating structure collapse phenomenon and preserving structure information. SDE accurately identifies hard samples and guides the model to prioritize optimizing these samples, mitigating their adverse impact on the latent space’s structure. Comprehensive experiments validate the superiority of our TopoFR.

## 7 Broader Impacts

It would be good to mention that the utilization of face images do not have any privacy concern given the datasets have proper license and users consent to distribute biometric data for research purpose. We address the well-defined face recognition task and conduct experiments on publicly available face datasets. Therefore, the propose method does not involve sensitive attributes and we do not notice any negative societal issues.

## References

- [1] Jiankang Deng, Jia Guo, Niannan Xue, and Stefanos Zafeiriou. Arcface: Additive angular margin loss for deep face recognition. In *Proceedings of the IEEE/CVF conference on computer vision and pattern recognition*, pages 4690–4699, 2019.
- [2] Hao Wang, Yitong Wang, Zheng Zhou, Xing Ji, Dihong Gong, Jingchao Zhou, Zhifeng Li, and Wei Liu. Cosface: Large margin cosine loss for deep face recognition. In *Proceedings of the IEEE conference on computer vision and pattern recognition*, pages 5265–5274, 2018.
- [3] Minchul Kim, Anil K Jain, and Xiaoming Liu. Adaface: Quality adaptive margin for face recognition. In *Proceedings of the IEEE/CVF Conference on Computer Vision and Pattern Recognition*, pages 18750–18759, 2022.
- [4] Yuge Huang, Yuhan Wang, Ying Tai, Xiaoming Liu, Pengcheng Shen, Shaoxin Li, Jilin Li, and Feiyue Huang. Curricularface: adaptive curriculum learning loss for deep face recognition. In *proceedings of the IEEE/CVF conference on computer vision and pattern recognition*, pages 5901–5910, 2020.
- [5] Qiang Meng, Shichao Zhao, Zhida Huang, and Feng Zhou. Magface: A universal representation for face recognition and quality assessment. In *Proceedings of the IEEE/CVF conference on computer vision and pattern recognition*, pages 14225–14234, 2021.
- [6] Jie Chang, Zhonghao Lan, Changmao Cheng, and Yichen Wei. Data uncertainty learning in face recognition. In *Proceedings of the IEEE/CVF conference on computer vision and pattern recognition*, pages 5710–5719, 2020.

- [7] Florian Schroff, Dmitry Kalenichenko, and James Philbin. Facenet: A unified embedding for face recognition and clustering. In *Proceedings of the IEEE conference on computer vision and pattern recognition*, pages 815–823, 2015.
- [8] Yaoyao Zhong and Weihong Deng. Face transformer for recognition. *arXiv preprint arXiv:2103.14803*, 2021.
- [9] Jun Dan, Yang Liu, Haoyu Xie, Jiankang Deng, Haoran Xie, Xuansong Xie, and Baigui Sun. Transface: Calibrating transformer training for face recognition from a data-centric perspective. In *Proceedings of the IEEE/CVF International Conference on Computer Vision*, pages 20642–20653, 2023.
- [10] Wenjie Zhu and Bo Peng. Manifold-based aggregation clustering for unsupervised vehicle re-identification. *Knowledge-Based Systems*, 235:107624, 2022.
- [11] Fan Wu, Hao Ma, Yun Guan, and Lixia Tian. Manifold-based unsupervised metric learning, with applications in individualized predictions based on functional connectivity. *Biomedical Signal Processing and Control*, 79:104081, 2023.
- [12] Kejie Jiang, Qiang Han, Xiuli Du, and Pinghe Ni. A decentralized unsupervised structural condition diagnosis approach using deep auto-encoders. *Computer-Aided Civil and Infrastructure Engineering*, 36(6):711–732, 2021.
- [13] Leonardo Tadeu Lopes and Daniel Carlos Guimarães Pedronette. Self-supervised clustering based on manifold learning and graph convolutional networks. In *Proceedings of the IEEE/CVF Winter Conference on Applications of Computer Vision*, pages 5634–5643, 2023.
- [14] Jun Dan, Tao Jin, Hao Chi, Yixuan Shen, Jiawang Yu, and Jinhai Zhou. Homda: High-order moment-based domain alignment for unsupervised domain adaptation. *Knowledge-Based Systems*, 261:110205, 2023.
- [15] Jun Dan, Weiming Liu, Mushui Liu, Chunfeng Xie, Shunjie Dong, Guofang Ma, Yanchao Tan, and Jiazheng Xing. Hogda: Boosting semi-supervised graph domain adaptation via high-order structure-guided adaptive feature alignmen. In *ACM Multimedia 2024*, 2024.
- [16] Chi-Chong Wong and Chi-Man Vong. Persistent homology based graph convolution network for fine-grained 3d shape segmentation. In *Proceedings of the IEEE/CVF International Conference on Computer Vision*, pages 7098–7107, 2021.
- [17] Qitian Wu, Chenxiao Yang, Wentao Zhao, Yixuan He, David Wipf, and Junchi Yan. Difformer: Scalable (graph) transformers induced by energy constrained diffusion. *arXiv preprint arXiv:2301.09474*, 2023.
- [18] Yuriy Mileyko, Sayan Mukherjee, and John Harer. Probability measures on the space of persistence diagrams. *Inverse Problems*, 27(12):124007, 2011.
- [19] Afra Zomorodian and Gunnar Carlsson. Computing persistent homology. In *Proceedings of the twentieth annual symposium on Computational geometry*, pages 347–356, 2004.
- [20] Herbert Edelsbrunner, John Harer, et al. Persistent homology-a survey. *Contemporary mathematics*, 453(26):257–282, 2008.
- [21] Serguei Barannikov. The framed morse complex and its invariants. *Advances in Soviet Mathematics*, 21:93–116, 1994.
- [22] Gunnar Carlsson. Topology and data. *Bulletin of the American Mathematical Society*, 46(2):255–308, 2009.
- [23] Brianna Maze, Jocelyn Adams, James A Duncan, Nathan Kalka, Tim Miller, Charles Otto, Anil K Jain, W Tyler Niggel, Janet Anderson, Jordan Cheney, et al. Iarpa janus benchmark-c: Face dataset and protocol. In *2018 international conference on biometrics (ICB)*, pages 158–165. IEEE, 2018.

[24] Jun Dan, Tao Jin, Hao Chi, Shunjie Dong, and Yixuan Shen. Uncertainty-guided joint unbalanced optimal transport for unsupervised domain adaptation. *Neural Computing and Applications*, 35(7):5351–5367, 2023.

[25] Shen Li, Jianqing Xu, Xiaqing Xu, Pengcheng Shen, Shaoxin Li, and Bryan Hooi. Spherical confidence learning for face recognition. In *Proceedings of the IEEE/CVF Conference on Computer Vision and Pattern Recognition*, pages 15629–15637, 2021.

[26] Yichun Shi and Anil K Jain. Probabilistic face embeddings. In *Proceedings of the IEEE/CVF International Conference on Computer Vision*, pages 6902–6911, 2019.

[27] Jiankang Deng, Jia Guo, Xiang An, Zheng Zhu, and Stefanos Zafeiriou. Masked face recognition challenge: The insightface track report. In *Proceedings of the IEEE/CVF International Conference on Computer Vision*, pages 1437–1444, 2021.

[28] Mushui Liu, Yunlong Yu, Zhong Ji, Jungong Han, and Zhongfei Zhang. Tolerant self-distillation for image classification. *Neural Networks*, 2024.

[29] Mushui Liu, Fangtai Wu, Bozheng Li, Ziqian Lu, Yunlong Yu, and Xi Li. Envisioning class entity reasoning by large language models for few-shot learning. In *AAAI*, 2025.

[30] Yang Liu, Fei Wang, Jiankang Deng, Zhipeng Zhou, Baigui Sun, and Hao Li. Mogface: Towards a deeper appreciation on face detection. In *Proceedings of the IEEE/CVF Conference on Computer Vision and Pattern Recognition*, pages 4093–4102, 2022.

[31] Yang Liu, Jiankang Deng, Fei Wang, Lei Shang, Xuansong Xie, and Baigui Sun. Damofd: Digging into backbone design on face detection. In *The Eleventh International Conference on Learning Representations*, 2022.

[32] Yang Liu, Xu Tang, Junyu Han, Jingtuo Liu, Dinger Rui, and Xiang Wu. Hambox: Delving into mining high-quality anchors on face detection. In *2020 IEEE/CVF Conference on Computer Vision and Pattern Recognition (CVPR)*, pages 13043–13051. IEEE, 2020.

[33] Yang Liu and Xu Tang. Bbbox: Searching face-appropriate backbone and feature pyramid network for face detector. In *Proceedings of the IEEE/CVF Conference on Computer Vision and Pattern Recognition*, pages 13568–13577, 2020.

[34] Jiankang Deng, Jia Guo, Evangelos Ververas, Irene Kotsia, and Stefanos Zafeiriou. Retinaface: Single-shot multi-level face localisation in the wild. In *Proceedings of the IEEE/CVF conference on computer vision and pattern recognition*, pages 5203–5212, 2020.

[35] Kihyuk Sohn. Improved deep metric learning with multi-class n-pair loss objective. *Advances in neural information processing systems*, 29, 2016.

[36] Yandong Wen, Kaipeng Zhang, Zhifeng Li, and Yu Qiao. A discriminative feature learning approach for deep face recognition. In *Computer Vision–ECCV 2016: 14th European Conference, Amsterdam, The Netherlands, October 11–14, 2016, Proceedings, Part VII 14*, pages 499–515. Springer, 2016.

[37] Feng Wang, Jian Cheng, Weiyang Liu, and Haijun Liu. Additive margin softmax for face verification. *IEEE Signal Processing Letters*, 25(7):926–930, 2018.

[38] Weiyang Liu, Yandong Wen, Zhiding Yu, Ming Li, Bhiksha Raj, and Le Song. Spherefafce: Deep hypersphere embedding for face recognition. In *Proceedings of the IEEE conference on computer vision and pattern recognition*, pages 212–220, 2017.

[39] Xingkun Xu, Yuge Huang, Pengcheng Shen, Shaoxin Li, Jilin Li, Feiyue Huang, Yong Li, and Zhen Cui. Consistent instance false positive improves fairness in face recognition. In *Proceedings of the IEEE/CVF conference on computer vision and pattern recognition*, pages 578–586, 2021.

[40] Jiankang Deng, Jia Guo, Tongliang Liu, Mingming Gong, and Stefanos Zafeiriou. Sub-center arcface: Boosting face recognition by large-scale noisy web faces. In *Computer Vision–ECCV 2020: 16th European Conference, Glasgow, UK, August 23–28, 2020, Proceedings, Part XI 16*, pages 741–757. Springer, 2020.

[41] Xiang An, Xuhan Zhu, Yuan Gao, Yang Xiao, Yongle Zhao, Ziyong Feng, Lan Wu, Bin Qin, Ming Zhang, Debing Zhang, et al. Partial fc: Training 10 million identities on a single machine. In *Proceedings of the IEEE/CVF International Conference on Computer Vision*, pages 1445–1449, 2021.

[42] Pengyu Li, Biao Wang, and Lei Zhang. Virtual fully-connected layer: Training a large-scale face recognition dataset with limited computational resources. In *Proceedings of the IEEE/CVF Conference on Computer Vision and Pattern Recognition*, pages 13315–13324, 2021.

[43] Xiang An, Jiankang Deng, Jia Guo, Ziyong Feng, XuHan Zhu, Jing Yang, and Tongliang Liu. Killing two birds with one stone: Efficient and robust training of face recognition cnns by partial fc. In *Proceedings of the IEEE/CVF Conference on Computer Vision and Pattern Recognition*, pages 4042–4051, 2022.

[44] Jose A Perea and John Harer. Sliding windows and persistence: An application of topological methods to signal analysis. *Foundations of Computational Mathematics*, 15:799–838, 2015.

[45] Christopher J Tralie and Jose A Perea. (quasi) periodicity quantification in video data, using topology. *SIAM Journal on Imaging Sciences*, 11(2):1049–1077, 2018.

[46] Mushui Liu, Bozheng Li, and Yunlong Yu. Omniclip: Adapting clip for video recognition with spatial-temporal omni-scale feature learning. ECAI, 2024.

[47] Gurjeet Singh, Facundo Memoli, Tigran Ishkhanov, Guillermo Sapiro, Gunnar Carlsson, and Dario L Ringach. Topological analysis of population activity in visual cortex. *Journal of vision*, 8(8):11–11, 2008.

[48] Yuri Dabaghian, Facundo Mémoli, Loren Frank, and Gunnar Carlsson. A topological paradigm for hippocampal spatial map formation using persistent homology. 2012.

[49] Yu-Min Chung, Chuan-Shen Hu, Austin Lawson, and Clifford Smyth. Topological approaches to skin disease image analysis. In *2018 IEEE International Conference on Big Data (Big Data)*, pages 100–105. IEEE, 2018.

[50] Bastian Rieck and Heike Leitte. Persistent homology for the evaluation of dimensionality reduction schemes. In *Computer Graphics Forum*, volume 34, pages 431–440. Wiley Online Library, 2015.

[51] Bastian Rieck and Heike Leitte. Agreement analysis of quality measures for dimensionality reduction. In *Topological Methods in Data Analysis and Visualization IV: Theory, Algorithms, and Applications VI*, pages 103–117. Springer, 2017.

[52] James R Clough, Nicholas Byrne, Ilkay Oksuz, Veronika A Zimmer, Julia A Schnabel, and Andrew P King. A topological loss function for deep-learning based image segmentation using persistent homology. *IEEE Transactions on Pattern Analysis and Machine Intelligence*, 44(12):8766–8778, 2020.

[53] Ekaterina Khramtsova, Guido Zuccon, Xi Wang, and Mahsa Baktashmotlagh. Rethinking persistent homology for visual recognition. In *Topological, Algebraic and Geometric Learning Workshops 2022*, pages 206–215. PMLR, 2022.

[54] Vinay Venkataraman, Karthikeyan Natesan Ramamurthy, and Pavan Turaga. Persistent homology of attractors for action recognition. In *2016 IEEE international conference on image processing (ICIP)*, pages 4150–4154. IEEE, 2016.

[55] Danijela Horak, Simiao Yu, and Gholamreza Salimi-Khorshidi. Topology distance: A topology-based approach for evaluating generative adversarial networks. In *Proceedings of the AAAI Conference on Artificial Intelligence*, volume 35, pages 7721–7728, 2021.

[56] Herbert Edelsbrunner, David Letscher, and Afra Zomorodian. Topological persistence and simplification. In *Proceedings 41st annual symposium on foundations of computer science*, pages 454–463. IEEE, 2000.

[57] Leopold Vietoris. Über den höheren zusammenhang kompakter räume und eine klasse von zusammenhangstreuen abbildungen. *Mathematische Annalen*, 97(1):454–472, 1927.

[58] Herbert Edelsbrunner. Persistent homology: theory and practice. 2013.

[59] David Cohen-Steiner, Herbert Edelsbrunner, and John Harer. Stability of persistence diagrams. In *Proceedings of the twenty-first annual symposium on Computational geometry*, pages 263–271, 2005.

[60] Katharine Turner, Yuriy Mileyko, Sayan Mukherjee, and John Harer. Fréchet means for distributions of persistence diagrams. *Discrete & Computational Geometry*, 52:44–70, 2014.

[61] Dimitri P Bertsekas. A new algorithm for the assignment problem. *Mathematical Programming*, 21(1):152–171, 1981.

[62] Afra Zomorodian. Fast construction of the vietoris-rips complex. *Computers & Graphics*, 34(3):263–271, 2010.

[63] David Cohen-Steiner, Herbert Edelsbrunner, and John Harer. Extending persistence using poincaré and lefschetz duality. *Foundations of Computational Mathematics*, 9(1):79–103, 2009.

[64] Michael Moor, Max Horn, Bastian Rieck, and Karsten Borgwardt. Topological autoencoders. In *International conference on machine learning*, pages 7045–7054. PMLR, 2020.

[65] Yichun Shi, Xiang Yu, Kihyuk Sohn, Manmohan Chandraker, and Anil K Jain. Towards universal representation learning for deep face recognition. In *Proceedings of the IEEE/CVF Conference on Computer Vision and Pattern Recognition*, pages 6817–6826, 2020.

[66] Jun Dan, Tao Jin, Hao Chi, Shunjie Dong, Haoran Xie, Keying Cao, and Xinjing Yang. Trust-aware conditional adversarial domain adaptation with feature norm alignment. *Neural Networks*, 168:518–530, 2023.

[67] Weiming Liu, Chaochao Chen, Xinting Liao, Mengling Hu, Jiajie Su, Yanchao Tan, and Fan Wang. User distribution mapping modelling with collaborative filtering for cross domain recommendation. In *Proceedings of the ACM on Web Conference 2024*, pages 334–343, 2024.

[68] Ziqian Lu, Fengli Shen, Mushui Liu, Yunlong Yu, and Xi Li. Improving zero-shot generalization for clip with variational adapter. *ECCV*, 2024.

[69] Weiming Liu, Xiaolin Zheng, Chaochao Chen, Jiajie Su, Xinting Liao, Mengling Hu, and Yanchao Tan. Joint internal multi-interest exploration and external domain alignment for cross domain sequential recommendation. In *Proceedings of the ACM Web Conference 2023*, pages 383–394, 2023.

[70] Weiming Liu, Xiaolin Zheng, Jiajie Su, Longfei Zheng, Chaochao Chen, and Mengling Hu. Contrastive proxy kernel stein path alignment for cross-domain cold-start recommendation. *IEEE Transactions on Knowledge and Data Engineering*, 35(11):11216–11230, 2023.

[71] Weiming Liu, Xiaolin Zheng, Jiajie Su, Mengling Hu, Yanchao Tan, and Chaochao Chen. Exploiting variational domain-invariant user embedding for partially overlapped cross domain recommendation. In *Proceedings of the 45th International ACM SIGIR conference on research and development in information retrieval*, pages 312–321, 2022.

[72] Olivier Chapelle and Alexander Zien. Semi-supervised classification by low density separation. In *International workshop on artificial intelligence and statistics*, pages 57–64. PMLR, 2005.

[73] Weiming Liu, Xiaolin Zheng, Mengling Hu, and Chaochao Chen. Collaborative filtering with attribution alignment for review-based non-overlapped cross domain recommendation. In *Proceedings of the ACM web conference 2022*, pages 1181–1190, 2022.

[74] Alessio De Angelis, Guido De Angelis, and Paolo Carbone. Using gaussian-uniform mixture models for robust time-interval measurement. *IEEE Transactions on Instrumentation and Measurement*, 64(12):3545–3554, 2015.

[75] Stéphane Lathuilière, Pablo Mesejo, Xavier Alameda-Pineda, and Radu Horaud. Deepgum: Learning deep robust regression with a gaussian-uniform mixture model. In *Proceedings of the European Conference on Computer Vision (ECCV)*, pages 202–217, 2018.

[76] Xiang Gu, Jian Sun, and Zongben Xu. Spherical space domain adaptation with robust pseudo-label loss. In *Proceedings of the IEEE/CVF conference on computer vision and pattern recognition*, pages 9101–9110, 2020.

[77] Bin Dai, Shilin Ding, and Grace Wahba. Multivariate bernoulli distribution. 2013.

[78] Pietro Coretto and Christian Hennig. Robust improper maximum likelihood: tuning, computation, and a comparison with other methods for robust gaussian clustering. *Journal of the American Statistical Association*, 111(516):1648–1659, 2016.

[79] Tsung-Yi Lin, Priya Goyal, Ross Girshick, Kaiming He, and Piotr Dollár. Focal loss for dense object detection. In *Proceedings of the IEEE international conference on computer vision*, pages 2980–2988, 2017.

[80] Zheng Zhu, Guan Huang, Jiankang Deng, Yun Ye, Junjie Huang, Xinze Chen, Jiagang Zhu, Tian Yang, Dalong Du, Jiwen Lu, et al. Webface260m: A benchmark for million-scale deep face recognition. *IEEE Transactions on Pattern Analysis and Machine Intelligence*, 45(2):2627–2644, 2022.

[81] Gary B Huang, Marwan Mattar, Tamara Berg, and Eric Learned-Miller. Labeled faces in the wild: A database for studying face recognition in unconstrained environments. In *Workshop on faces in 'Real-Life' Images: detection, alignment, and recognition*, 2008.

[82] Stylianos Moschoglou, Athanasios Papaioannou, Christos Sagonas, Jiankang Deng, Irene Kotsia, and Stefanos Zafeiriou. Agedb: the first manually collected, in-the-wild age database. In *proceedings of the IEEE conference on computer vision and pattern recognition workshops*, pages 51–59, 2017.

[83] Soumyadip Sengupta, Jun-Cheng Chen, Carlos Castillo, Vishal M Patel, Rama Chellappa, and David W Jacobs. Frontal to profile face verification in the wild. In *2016 IEEE winter conference on applications of computer vision (WACV)*, pages 1–9. IEEE, 2016.

[84] Tianyue Zheng and Weihong Deng. Cross-pose lfw: A database for studying cross-pose face recognition in unconstrained environments. *Beijing University of Posts and Telecommunications, Tech. Rep.*, 5(7):5, 2018.

[85] Tianyue Zheng, Weihong Deng, and Jian Hu. Cross-age lfw: A database for studying cross-age face recognition in unconstrained environments. *arXiv preprint arXiv:1708.08197*, 2017.

[86] Cameron Whitelam, Emma Taborsky, Austin Blanton, Brianna Maze, Jocelyn Adams, Tim Miller, Nathan Kalka, Anil K Jain, James A Duncan, Kristen Allen, et al. Iarpa janus benchmark-b face dataset. In *proceedings of the IEEE conference on computer vision and pattern recognition workshops*, pages 90–98, 2017.

[87] Jiancan Zhou, Xi Jia, Qiufu Li, Linlin Shen, and Jinming Duan. Uniface: Unified cross-entropy loss for deep face recognition. In *Proceedings of the IEEE/CVF International Conference on Computer Vision*, pages 20730–20739, 2023.

[88] Xiaobo Wang, Shifeng Zhang, Shuo Wang, Tianyu Fu, Hailin Shi, and Tao Mei. Mis-classified vector guided softmax loss for face recognition. In *Proceedings of the AAAI Conference on Artificial Intelligence*, volume 34, pages 12241–12248, 2020.

[89] Yonghyun Kim, Wonpyo Park, and Jongju Shin. Broadface: Looking at tens of thousands of people at once for face recognition. In *Computer Vision–ECCV 2020: 16th European Conference, Glasgow, UK, August 23–28, 2020, Proceedings, Part IX*, pages 536–552. Springer, 2020.

[90] Jiaheng Liu, Yudong Wu, Yichao Wu, Chuming Li, Xiaolin Hu, Ding Liang, and Mengyu Wang. Dam: Discrepancy alignment metric for face recognition. In *Proceedings of the IEEE/CVF International Conference on Computer Vision*, pages 3814–3823, 2021.

- [91] Fadi Boutros, Naser Damer, Florian Kirchbuchner, and Arjan Kuijper. Elasticface: Elastic margin loss for deep face recognition. In *Proceedings of the IEEE/CVF Conference on Computer Vision and Pattern Recognition (CVPR) Workshops*, pages 1578–1587, June 2022.
- [92] Kaiming He, Xiangyu Zhang, Shaoqing Ren, and Jian Sun. Deep residual learning for image recognition. In *Proceedings of the IEEE conference on computer vision and pattern recognition*, pages 770–778, 2016.
- [93] Yuanqing Huang, Yinggui Wang, Le Yang, and Lei Wang. Enhanced face recognition using intra-class incoherence constraint. In *The Twelfth International Conference on Learning Representations*, 2023.
- [94] Sheng Chen, Yang Liu, Xiang Gao, and Zhen Han. Mobilefacenets: Efficient cnns for accurate real-time face verification on mobile devices. In *Biometric Recognition: 13th Chinese Conference, CCBR 2018, Urumqi, China, August 11-12, 2018, Proceedings 13*, pages 428–438. Springer, 2018.
- [95] Yanbo Fan, Siwei Lyu, Yiming Ying, and Baogang Hu. Learning with average top-k loss. *Advances in neural information processing systems*, 30, 2017.
- [96] Anirudh Som, Kowshik Thopalli, Karthikeyan Natesan Ramamurthy, Vinay Venkataraman, Ankita Shukla, and Pavan Turaga. Perturbation robust representations of topological persistence diagrams. In *Proceedings of the European Conference on Computer Vision (ECCV)*, pages 617–635, 2018.
- [97] Matthew Kahle. Random geometric complexes. *Discrete & Computational Geometry*, 45:553–573, 2011.
- [98] Omer Bobrowski and Matthew Kahle. Topology of random geometric complexes: a survey. *Journal of applied and Computational Topology*, 1:331–364, 2018.

## A Appendix

### A.1 Implementation Details

**Training Details.** For MS1MV2 and Glint360K, our models are trained using Pytorch on 4 NVIDIA Tesla A100 GPUs, and a mini-batch of 128 images is assigned for each GPU. In the case of WebFace42M, we train our models (ResNet-200 backbone) using 64 NVIDIA Tesla V100 GPUs. We crop all images to  $112 \times 112$ , following the same setting as in ArcFace [1, 34]. For the backbones, we adopt ResNet-50, ResNet-100 and ResNet-200 [92] as modified in [1]. We follow [1] to employ ArcFace ( $s = 64$  and  $m = 0.5$ ) as the basic classification loss to train the TopoFR model. For the TopoFR $^\dagger$  model trained by CosFace [2], we set the scale  $s$  to 64 and the cosine margin  $m$  of CosFace to 0.4. To optimize the models, we use Stochastic Gradient Descent (SGD) optimizer with momentum of 0.9 for both datasets. The weight decay for MS1MV2 is set to 5e-4 and 1e-4 for Glint360K. The initial learning rate is set to 0.1 for both datasets. In terms of the balance coefficient  $\alpha$ , we choose  $\alpha = 0.1$  for experiments on R50 TopoFR, and  $\alpha = 0.05$  for experiments on R100 TopoFR and R200 TopoFR. During training, we apply RSP mechanism with a certain probability. Specially, for an original input sample  $x$ , the probability of it undergoing RSP is  $\xi$ , and the probability of it remaining unchanged is  $1 - \xi$ . For the hyper-parameter  $\xi$ , we choose  $\xi = 0.2$ . Notably, in our method, we focus on preserving the 0-dimension homology  $H_0$  in the topological structure alignment loss  $\mathcal{L}_{sa}$ . Because preliminary experiments demonstrated that using the 1-dimension or higher-dimension homology only increases model’s training time without clear performance gains. Code and pre-trained models are available at: [https://github.com/modelscope/facechain/tree/main/face\\_module/TopoFR](https://github.com/modelscope/facechain/tree/main/face_module/TopoFR).

**Evaluation Protocol on MFR-Ongoing Challenge.** In the MFR-Ongoing Challenge, the trained models are submitted to and evaluated by the online server. Specially, "TAR@FAR=1e-4" and "TAR@FAR=1e-5" are reported on the IJB-C. Furthermore, we report "TAR@FAR=1e-4" for Mask and Children test sets, and "TAR@FAR=1e-6" for MR-ALL test set. The academic track of the ongoing MFR challenge leaderboard can be found on <http://iccv21-mfr.com/#/leaderboard/academic>. More details about the MFR-Ongoing Challenge can be found in Ref. [27].

### A.2 More Results

#### A.2.1 Experiments on Other Benchmarks

**Results on CPLFW and CALFW.** We utilize MS1MV2 as the training set, and compare our TopoFR with SOTA methods on CPLFW and CALFW benchmarks, as reported in 4. As can be seen, the proposed R50 TopoFR and R50 TopoFR $^\dagger$  greatly outperform the SOTA competitor R50 AdaFace on two benchmarks. Furthermore, under the ResNet-100 backbone, our TopoFR also achieves SOTA performance and surpasses AdaFace by 0.26% and 0.36% on CPLFW and CALFW respectively.

Table 4: Verification accuracy (%) on CPLFW and CALFW.

Training Data	Method	Venue	CPLFW	CALFW
MS1MV2	R50, ArcFace [1]	CVPR19	91.76	95.14
	R50, MagFace [5]	CVPR21	92.49	95.88
	R50, AdaFace [3]	CVPR22	92.83	96.07
	R50, <b>TopoFR</b> $^\dagger$	NeurIPS24	93.36	96.24
	R50, <b>TopoFR</b>	NeurIPS24	<b>93.38</b>	<b>96.25</b>
	R100, CosFace [2]	CVPR18	92.26	95.75
	R100, ArcFace [1]	CVPR19	92.10	95.47
	R100, MV-Softmax [88]	AAAI20	92.83	96.10
	R100, BroadFace [89]	ECCV20	93.17	96.20
	R100, CurricularFace [4]	CVPR20	93.13	96.20
	R100, MagFace [5]	CVPR21	92.87	96.15
	R100, SCF-ArcFace [25]	CVPR21	93.16	96.12
	R100, ElasticFace-Arc+ [91]	CVPR22	93.28	96.17
	R100, ElasticFace-Cos+ [91]	CVPR22	93.23	96.18
	R100, AdaFace [3]	CVPR22	93.53	96.08
	R100, IIC-AdaFace [93]	ICLR24	93.48	96.18
	R100, <b>TopoFR</b> $^\dagger$	NeurIPS24	93.78	96.42
	R100, <b>TopoFR</b>	NeurIPS24	<b>93.79</b>	<b>96.44</b>

### A.2.2 Experiments on Light-weight Network

To demonstrate the universality of our method, we conduct some experiments on a lightweight network MobileFaceNet-0.45G [94], as shown in Table 5. We can observe that with the help of SDE and PTSAs strategies, the MobileFaceNet-0.45G model can achieve higher recognition accuracy, implying the effectiveness and universality of our method.

Table 5: Verification performance (%) on IJB-C. MobileFaceNet refers to the MobileFaceNet-0.45G backbone [94].

Training Data	Method	IJB-C (1e-6)	IJB-C (1e-5)	IJB-C (1e-4)
MS1MV2	MobileFaceNet	81.75	90.13	93.42
MS1MV2	MobileFaceNet + PTSAs + SDE	<b>83.14</b>	<b>91.01</b>	<b>94.48</b>
Glint360K	MobileFaceNet	83.67	92.49	94.86
Glint360K	MobileFaceNet + PTSAs + SDE	<b>85.44</b>	<b>93.35</b>	<b>95.79</b>

### A.3 More Ablation Experiments and Analysis

**1) Does Structure Information Improve Intra-class and Inter-class Relationships?:** We conduct two pairs of ablative experiments to validate the relationships between topological structure alignment and intra-class distance constraint as well as inter-class distance constraint. The results are gathered in Table 6.

We can find that integrating topological structure alignment with single inter-class or intra-class distance constraint can both obtain additional significant performance gains. This indicates that topological structure alignment can provide the extra structure information of intra-class and inter-class relationships, thereby establishing clearer decision boundaries. Overall, these improved results demonstrate topological structure alignment implicitly encourages intra-class compactness and inter-class separability in the deep feature space.

Table 6: Verification performance (%) on IJB-C. Relationships between Topological Structure Information and Intra-class/ Inter-class constraints.

Training Data	Method	IJB-C (1e-6)	IJB-C (1e-5)	IJB-C (1e-4)
MS1MV2	R100, ArcFace (w/o intra-class)	82.37	89.13	94.16
	R100, ArcFace(w/o intra-class) + topological constraint	<b>83.69</b>	<b>91.48</b>	<b>94.86</b>
MS1MV2	R100, ArcFace(w/o inter-class)	82.72	89.51	94.47
	R100, ArcFace(w/o inter-class) + topological constraint	<b>84.53</b>	<b>92.36</b>	<b>95.12</b>

**2) Comparison with Previous Hard Sample Mining Strategies:** To further demonstrate the superiority of our SDE strategy in mining hard samples, we compare it with existing hard sample mining strategies, including MV-Softmax [88], AT<sub>k</sub> [95] loss, Focal loss [79] and the recently proposed EHSM [9].

The results are gathered in Table 7. We can observe that the proposed SDE strategy clearly outperforms than previous hard sample mining strategies, indicating that our SDE strategy is better able to measure sample difficulty and improve the model’s generalization performance. This is because the SDE comprehensively considers the prediction uncertainty and label information (*i.e.*, prediction probability of ground truth) when mining hard samples.

**3) Effectiveness of ISA:** Previous works often use Bottleneck distance and p-Wasserstein distance to measure the distance between persistence diagrams  $\mathcal{D}^{\mathcal{X}}$  and  $\mathcal{D}^{\tilde{\mathcal{Z}}}$  [18, 60]. Concretely, the Bottleneck distance is defined as  $\mathcal{L}_{\infty}(\mathcal{D}^{\mathcal{X}}, \mathcal{D}^{\tilde{\mathcal{Z}}}) = \inf_{\kappa: \mathcal{D}^{\mathcal{X}} \rightarrow \mathcal{D}^{\tilde{\mathcal{Z}}}} \sup_{\varpi \in \mathcal{D}^{\mathcal{X}}} \|\varpi - \kappa(\varpi)\|_{\infty}$ , with  $\kappa$  ranging over all bijections between sets of persistent intervals in diagrams  $\mathcal{D}^{\mathcal{X}}$  and  $\mathcal{D}^{\tilde{\mathcal{Z}}}$ , and  $\|\cdot\|_{\infty}$  denotes the  $\infty$ -norm. Equivalently, the p-Wasserstein distance is defined as  $\mathcal{L}_p(\mathcal{D}^{\mathcal{X}}, \mathcal{D}^{\tilde{\mathcal{Z}}}) = (\inf_{\kappa: \mathcal{D}^{\mathcal{X}} \rightarrow \mathcal{D}^{\tilde{\mathcal{Z}}}} \sum_{\varpi \in \mathcal{D}^{\mathcal{X}}} \|\varpi - \kappa(\varpi)\|_{\infty}^p)^{1/p}$ . However, the Bottleneck distance metric and p-Wasserstein distance metric are sensitive to outliers [55, 61, 96] and will significantly increase the training time of FR models. This makes them unsuitable for FR tasks with extremely large-scale datasets.

Table 7: Comparison with Previous Hard Sample Mining Strategies.

Training Data	Method	IJB-C (1e-6)	IJB-C (1e-5)	IJB-C (1e-4)
MS1MV2	R100, ArcFace	85.65	92.69	95.74
	R100, ArcFace + AT <sub>k</sub>	85.93	93.04	95.89
	R100, ArcFace + MV-Softmax	86.47	93.38	95.94
	R100, ArcFace + Focal Loss	87.58	93.87	96.11
	R100, ArcFace + EHSM	88.30	94.19	96.18
	R100, ArcFace + <b>SDE</b>	<b>89.23</b>	<b>94.65</b>	<b>96.49</b>

Table 8: Comparison of TopoFR using Different Metrics.

Training Data	Method	Average Training Time / Epoch	IJB-C (1e-4)
MS1MV2	R100, TopoFR-B	4312.56s	96.76
	R100, TopoFR-W	4127.29s	96.81
	<b>TopoFR</b>	<b>2729.28s</b>	<b>96.95</b>

To demonstrate the stability and computational efficiency of our ISA strategy, we employ MS1MV2 as the training set, and compare TopoFR and its two variants on the IJB-C benchmark. The variants of TopoFR are as follows: (1) **TopoFR-B**, the variant uses Bottleneck distance to compute the discrepancy between persistence diagrams. (2) **TopoFR-W**, the variant adopts 1-Wasserstein distance to measure the discrepancy between persistence diagrams.

We provide the average training time per epoch of these models and their recognition performance on "TAR@FAR=1e-4" of the IJB-C benchmarks. The results presented in Table 8 reflect the following observations: (1) TopoFR outperforms TopoFR-B and TopoFR-W on "TAR@FAR=1e-4", indicating the robustness of our ISA to outliers. (2) Compared with TopoFR-B and TopoFR-W, our proposed TopoFR has a shorter training time, demonstrating the computational efficiency of ISA.

**4) Effect of Batch Size:** We investigate the model's performance under different batch size, and the results are gathered in Table 9.

We find that increasing the batch size does not lead to a significant improvement in model's recognition accuracy. Additionally, larger batch size imposes a greater workload on GPUs. Therefore, to strike a balance between model's accuracy and GPU computational load, we choose to set the batch size to 128 in our TopoFR model.

Table 9: The Performance of TopoFR Model Under Different Batch Size.

Training Data	Method	Batch Size	IJB-C (1e-5)	IJB-C (1e-4)
MS1MV2	R100, TopoFR	128	<b>95.23</b>	<b>96.95</b>
	R100, TopoFR	256	95.22	96.91
	R100, TopoFR	512	95.20	96.93

**5) Training Time:** For detailed training time analysis, please refer to the Table 10. Due to the introduction of the structure alignment strategy PTSA and hard sample mining strategy SDE, our TopoFR models require longer training time (1.16x). Specially, compared to the vanilla R50 ArcFace model, our R50 TopoFR model requires about 2 seconds more training time per 100 steps, which does not significantly increase the training time but brings a large performance gain. And our R100 topoFR model requires about 3 seconds extra training time per 100 steps than the vanilla R100 ArcFace model, which is not a major increase in training time but leads to a significant performance advantage.

While for inference computation head, our method performs consistently with that of vanilla ArcFace model, since we adopt the same network architecture and data pre-process module.

Moreover, the results in Table 10 indicate that introducing SDE strategy (*i.e.*, GUM) leads to significant performance improvements with only a small increase in training time (*i.e.*, R50 backbone: 0.2s / 100 steps, R100 backbone: 0.25s / 100 steps), which is reasonable. Therefore, the addition of GUM does not bring too much computational burden and does not significantly increase the training time.

Table 10: Detailed Training Time of FR models.

Training Data	Method	Average Training Time / 100 steps	Average Training Time / Epoch	IJB-C (1e-4)
MS1MV2	R50, ArcFace	15.33s	1743.32s	92.52
	R50, ArcFace + PTSAs	17.57s	1999.19s	96.25
	R50, ArcFace + PTSAs + SDE ( <b>R50, TopoFR</b> )	17.77s	2020.80s	<b>96.49</b>
MS1MV2	R100, ArcFace	20.16s	2292.59s	95.74
	R100, ArcFace + PTSAs	23.10s	2626.93s	96.68
	R100, ArcFace + PTSAs + SDE ( <b>R100, TopoFR</b> )	23.35s	2655.36s	<b>96.95</b>

**6) Parameter Sensitivity:** To demonstrate the effect of the hyper-parameters  $\alpha$  (*i.e.*, the balance coefficient of the ISA loss  $\mathcal{L}_{sa}$ ) and  $\xi$  (*i.e.*, the probability of RSP mechanism), we conduct additional experiments by setting different values of  $\alpha$  and  $\xi$ , respectively. We use MS1MV2 dataset to train the R50 TopoFR and R100 TopoFR models, and evaluate their performance on the IJB-C benchmark. The results on "TAR@FAR=1e-4" are shown in Figures 6a and 6b.

We can observe that as  $\alpha$  increases, the accuracy first rises and then falls. This is because an overly large  $\alpha$  will cause the model to focus more on the structure alignment and less on the classification learning of the samples during training. Additionally, setting the parameter  $\xi$  to a high value may introduce more unidentifiable face images and severely disturb the topological structure of the latent space, making it difficult for the ISA loss function  $\mathcal{L}_{sa}$  to converge.

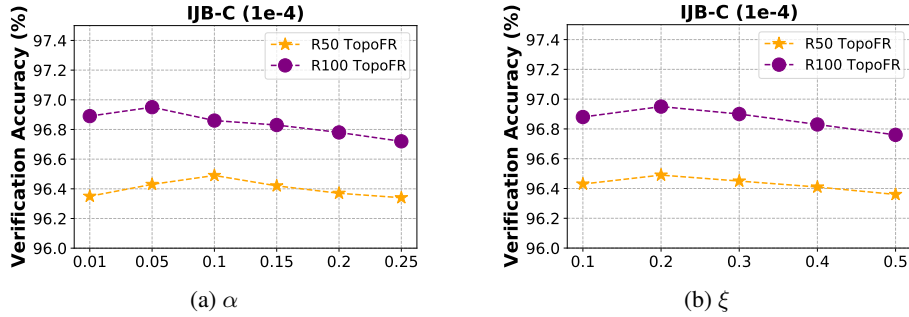


Figure 6: Parameter sensitivity analysis. (a) The effect of the hyper-parameter  $\alpha$ . (b) The effect of the hyper-parameter  $\xi$ .

**7) Comparison of Structure Discrepancy:** To further demonstrate the effectiveness of our PTSAs strategy in preserving structure information, we utilize the **Bottleneck distance metric** [60, 18] to investigate the topological structure discrepancy between the input space and the latent space of ArcFace and TopoFR on IJB-C benchmark, as illustrated in Figure 7.

We can observe that our TopoFR model significantly reduces the structure discrepancy (*i.e.*, measured by the Bottleneck distance metric) between two spaces compared to the vanilla ArcFace model, and effectively preserves the structure information hidden in the large-scale dataset.

**8) Visualization of Hard Samples:** We conduct a visual comparison experiment to visualize some hard samples that can be correctly classified by our method but cannot be correctly classified by existing method.

The visualization results illustrated in Figure 8 reflect the following observations: **(1)** Hard samples are usually blurry, low-contrast, occluded, or in unusual poses, so they are easily misclassified by existing method such as ArcFace model. **(2)** The ArcFace model assigns equal weight (*i.e.*, 1) to each sample. While our TopoFR model utilizes SDE strategy to adaptively assign weight (*i.e.*, SDS  $\omega$ ) to each sample based on its prediction uncertainty  $\omega_1$  and prediction accuracy  $\omega_2$ . Specially, SDE will assign higher SDS  $\omega$  to hard samples, which can encourage the model to extract robust face features from these challenging samples, thereby effectively improving the model's generalization performance.

**9) Is the topological structure constructed in the input space robust enough?** **i)** In the input space, we first flatten the face images into vector features and then calculate their pair-wise distance matrix in order to construct Vietoris-Rips complex. And the dimension of face features in the pixel space is significantly higher than that of the features in the latent layer space. Notably, the expected  $k$ -th

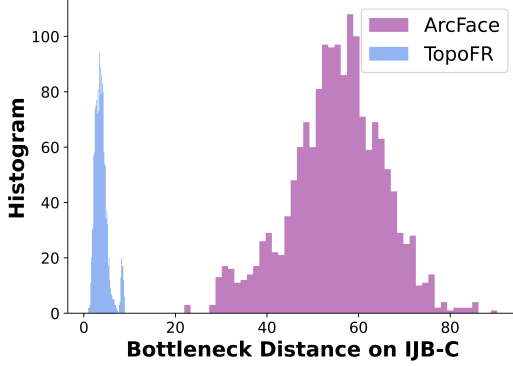


Figure 7: The topological structure discrepancy (*i.e.*, measured by the **Bottleneck distance metric**) of R50 TopoFR and R50 ArcFace on the IJB-C benchmark.



Figure 8: Visualization of hard samples.

Betti number  $\mathbb{E} [\beta_k^{VR}(r)] = c_k n (nr^d)^{2k+1}$  ( $n$ : data size,  $d$ : data dimension,  $c_k$ : constant) [97, 98] in topology theory also demonstrates that as long as the dimension of the data is sufficiently high, its underlying topological structure can be well constructed. Therefore, this can effectively capture the topological structure information hidden in the large-scale face datasets. **ii)** More importantly, during training, our RSP mechanism also effectively simulates the influence of multiple factors, such as lighting, occlusion, blur, etc., on the training samples, making the constructed topological structure robust enough to noise.

Overall, based on the analysis above, we believe that the topological structure constructed in the input space is sufficiently robust and can effectively guide the learning of the latent space structure.

#### A.4 Limitation

Our model might have the following two limitations:

- (i)** Due to the introduction of the structure alignment strategy PTSA and hard sample mining strategy SDE, our TopoFR model requires longer training time (1.16x). For detailed training time analysis, please refer to the Table 10 in our appendix.
- (ii)** This work aims to improve the generalization performance of FR models by leveraging the inherent structure information in large-scale face training data. However, large-scale face training datasets in real-world scenarios inevitably contain a small amount of noisy labels. Our loss function does not assign any special treatment to these mislabeled samples. Since our hard sample mining strategy SDE assigns larger weights to hard samples that are misclassified or have high prediction uncertainty, mislabeled images may be wrongly emphasized. We believe that future works will be able to simultaneously address the challenges of structure alignment and label noise.

## NeurIPS Paper Checklist

### 1. Claims

Question: Do the main claims made in the abstract and introduction accurately reflect the paper's contributions and scope?

Answer: **[Yes]**

Justification: The abstract and introduction section include the main claims made in the paper.

Guidelines:

- The answer NA means that the abstract and introduction do not include the claims made in the paper.
- The abstract and/or introduction should clearly state the claims made, including the contributions made in the paper and important assumptions and limitations. A No or NA answer to this question will not be perceived well by the reviewers.
- The claims made should match theoretical and experimental results, and reflect how much the results can be expected to generalize to other settings.
- It is fine to include aspirational goals as motivation as long as it is clear that these goals are not attained by the paper.

### 2. Limitations

Question: Does the paper discuss the limitations of the work performed by the authors?

Answer: **[Yes]**

Justification: We have discussed the limitations of this work. Please refer to the Section A.4 in the Appendix.

Guidelines:

- The answer NA means that the paper has no limitation while the answer No means that the paper has limitations, but those are not discussed in the paper.
- The authors are encouraged to create a separate "Limitations" section in their paper.
- The paper should point out any strong assumptions and how robust the results are to violations of these assumptions (e.g., independence assumptions, noiseless settings, model well-specification, asymptotic approximations only holding locally). The authors should reflect on how these assumptions might be violated in practice and what the implications would be.
- The authors should reflect on the scope of the claims made, e.g., if the approach was only tested on a few datasets or with a few runs. In general, empirical results often depend on implicit assumptions, which should be articulated.
- The authors should reflect on the factors that influence the performance of the approach. For example, a facial recognition algorithm may perform poorly when image resolution is low or images are taken in low lighting. Or a speech-to-text system might not be used reliably to provide closed captions for online lectures because it fails to handle technical jargon.
- The authors should discuss the computational efficiency of the proposed algorithms and how they scale with dataset size.
- If applicable, the authors should discuss possible limitations of their approach to address problems of privacy and fairness.
- While the authors might fear that complete honesty about limitations might be used by reviewers as grounds for rejection, a worse outcome might be that reviewers discover limitations that aren't acknowledged in the paper. The authors should use their best judgment and recognize that individual actions in favor of transparency play an important role in developing norms that preserve the integrity of the community. Reviewers will be specifically instructed to not penalize honesty concerning limitations.

### 3. Theory Assumptions and Proofs

Question: For each theoretical result, does the paper provide the full set of assumptions and a complete (and correct) proof?

Answer: [NA]

Justification: This work does not involve any novel theoretical findings.

Guidelines:

- The answer NA means that the paper does not include theoretical results.
- All the theorems, formulas, and proofs in the paper should be numbered and cross-referenced.
- All assumptions should be clearly stated or referenced in the statement of any theorems.
- The proofs can either appear in the main paper or the supplemental material, but if they appear in the supplemental material, the authors are encouraged to provide a short proof sketch to provide intuition.
- Inversely, any informal proof provided in the core of the paper should be complemented by formal proofs provided in appendix or supplemental material.
- Theorems and Lemmas that the proof relies upon should be properly referenced.

#### 4. Experimental Result Reproducibility

Question: Does the paper fully disclose all the information needed to reproduce the main experimental results of the paper to the extent that it affects the main claims and/or conclusions of the paper (regardless of whether the code and data are provided or not)?

Answer: [Yes]

Justification: We have provided the required code and pre-trained model for this paper. Please refer to the GitHub link provided at the end of the abstract.

Guidelines:

- The answer NA means that the paper does not include experiments.
- If the paper includes experiments, a No answer to this question will not be perceived well by the reviewers: Making the paper reproducible is important, regardless of whether the code and data are provided or not.
- If the contribution is a dataset and/or model, the authors should describe the steps taken to make their results reproducible or verifiable.
- Depending on the contribution, reproducibility can be accomplished in various ways. For example, if the contribution is a novel architecture, describing the architecture fully might suffice, or if the contribution is a specific model and empirical evaluation, it may be necessary to either make it possible for others to replicate the model with the same dataset, or provide access to the model. In general, releasing code and data is often one good way to accomplish this, but reproducibility can also be provided via detailed instructions for how to replicate the results, access to a hosted model (e.g., in the case of a large language model), releasing of a model checkpoint, or other means that are appropriate to the research performed.
- While NeurIPS does not require releasing code, the conference does require all submissions to provide some reasonable avenue for reproducibility, which may depend on the nature of the contribution. For example
  - (a) If the contribution is primarily a new algorithm, the paper should make it clear how to reproduce that algorithm.
  - (b) If the contribution is primarily a new model architecture, the paper should describe the architecture clearly and fully.
  - (c) If the contribution is a new model (e.g., a large language model), then there should either be a way to access this model for reproducing the results or a way to reproduce the model (e.g., with an open-source dataset or instructions for how to construct the dataset).
  - (d) We recognize that reproducibility may be tricky in some cases, in which case authors are welcome to describe the particular way they provide for reproducibility. In the case of closed-source models, it may be that access to the model is limited in some way (e.g., to registered users), but it should be possible for other researchers to have some path to reproducing or verifying the results.

#### 5. Open access to data and code

Question: Does the paper provide open access to the data and code, with sufficient instructions to faithfully reproduce the main experimental results, as described in supplemental material?

Answer: **[Yes]**

Justification: We have provided detailed implementation details (*i.e.*, Section A.1 in the Appendix) and provided the data and source code.

Guidelines:

- The answer NA means that paper does not include experiments requiring code.
- Please see the NeurIPS code and data submission guidelines (<https://nips.cc/public/guides/CodeSubmissionPolicy>) for more details.
- While we encourage the release of code and data, we understand that this might not be possible, so “No” is an acceptable answer. Papers cannot be rejected simply for not including code, unless this is central to the contribution (e.g., for a new open-source benchmark).
- The instructions should contain the exact command and environment needed to run to reproduce the results. See the NeurIPS code and data submission guidelines (<https://nips.cc/public/guides/CodeSubmissionPolicy>) for more details.
- The authors should provide instructions on data access and preparation, including how to access the raw data, preprocessed data, intermediate data, and generated data, etc.
- The authors should provide scripts to reproduce all experimental results for the new proposed method and baselines. If only a subset of experiments are reproducible, they should state which ones are omitted from the script and why.
- At submission time, to preserve anonymity, the authors should release anonymized versions (if applicable).
- Providing as much information as possible in supplemental material (appended to the paper) is recommended, but including URLs to data and code is permitted.

## 6. Experimental Setting/Details

Question: Does the paper specify all the training and test details (e.g., data splits, hyper-parameters, how they were chosen, type of optimizer, etc.) necessary to understand the results?

Answer: **[Yes]**

Justification: We have provided detailed implementation details (*i.e.*, Section A.1 in the Appendix) and provided the data and source code.

Guidelines:

- The answer NA means that the paper does not include experiments.
- The experimental setting should be presented in the core of the paper to a level of detail that is necessary to appreciate the results and make sense of them.
- The full details can be provided either with the code, in appendix, or as supplemental material.

## 7. Experiment Statistical Significance

Question: Does the paper report error bars suitably and correctly defined or other appropriate information about the statistical significance of the experiments?

Answer: **[No]**

Justification: We follow the standard experimental principles of previous FR works and report the best results.

Guidelines:

- The answer NA means that the paper does not include experiments.
- The authors should answer “Yes” if the results are accompanied by error bars, confidence intervals, or statistical significance tests, at least for the experiments that support the main claims of the paper.

- The factors of variability that the error bars are capturing should be clearly stated (for example, train/test split, initialization, random drawing of some parameter, or overall run with given experimental conditions).
- The method for calculating the error bars should be explained (closed form formula, call to a library function, bootstrap, etc.)
- The assumptions made should be given (e.g., Normally distributed errors).
- It should be clear whether the error bar is the standard deviation or the standard error of the mean.
- It is OK to report 1-sigma error bars, but one should state it. The authors should preferably report a 2-sigma error bar than state that they have a 96% CI, if the hypothesis of Normality of errors is not verified.
- For asymmetric distributions, the authors should be careful not to show in tables or figures symmetric error bars that would yield results that are out of range (e.g. negative error rates).
- If error bars are reported in tables or plots, The authors should explain in the text how they were calculated and reference the corresponding figures or tables in the text.

## 8. Experiments Compute Resources

Question: For each experiment, does the paper provide sufficient information on the computer resources (type of compute workers, memory, time of execution) needed to reproduce the experiments?

Answer: [\[Yes\]](#)

Justification: We have provided detailed implementation details and training settings (*i.e.*, Section A.1 in the Appendix)

Guidelines:

- The answer NA means that the paper does not include experiments.
- The paper should indicate the type of compute workers CPU or GPU, internal cluster, or cloud provider, including relevant memory and storage.
- The paper should provide the amount of compute required for each of the individual experimental runs as well as estimate the total compute.
- The paper should disclose whether the full research project required more compute than the experiments reported in the paper (e.g., preliminary or failed experiments that didn't make it into the paper).

## 9. Code Of Ethics

Question: Does the research conducted in the paper conform, in every respect, with the NeurIPS Code of Ethics <https://neurips.cc/public/EthicsGuidelines>?

Answer: [\[Yes\]](#)

Justification: The research conducted in the paper fully adheres to the NeurIPS Code of Ethics.

Guidelines:

- The answer NA means that the authors have not reviewed the NeurIPS Code of Ethics.
- If the authors answer No, they should explain the special circumstances that require a deviation from the Code of Ethics.
- The authors should make sure to preserve anonymity (e.g., if there is a special consideration due to laws or regulations in their jurisdiction).

## 10. Broader Impacts

Question: Does the paper discuss both potential positive societal impacts and negative societal impacts of the work performed?

Answer: [\[NA\]](#)

Justification: It would be good to mention the utilization of face images do not have any privacy concern given the datasets have proper license and users consent to distribute biometric data for research purpose.

Guidelines:

- The answer NA means that there is no societal impact of the work performed.
- If the authors answer NA or No, they should explain why their work has no societal impact or why the paper does not address societal impact.
- Examples of negative societal impacts include potential malicious or unintended uses (e.g., disinformation, generating fake profiles, surveillance), fairness considerations (e.g., deployment of technologies that could make decisions that unfairly impact specific groups), privacy considerations, and security considerations.
- The conference expects that many papers will be foundational research and not tied to particular applications, let alone deployments. However, if there is a direct path to any negative applications, the authors should point it out. For example, it is legitimate to point out that an improvement in the quality of generative models could be used to generate deepfakes for disinformation. On the other hand, it is not needed to point out that a generic algorithm for optimizing neural networks could enable people to train models that generate Deepfakes faster.
- The authors should consider possible harms that could arise when the technology is being used as intended and functioning correctly, harms that could arise when the technology is being used as intended but gives incorrect results, and harms following from (intentional or unintentional) misuse of the technology.
- If there are negative societal impacts, the authors could also discuss possible mitigation strategies (e.g., gated release of models, providing defenses in addition to attacks, mechanisms for monitoring misuse, mechanisms to monitor how a system learns from feedback over time, improving the efficiency and accessibility of ML).

## 11. Safeguards

Question: Does the paper describe safeguards that have been put in place for responsible release of data or models that have a high risk for misuse (e.g., pretrained language models, image generators, or scraped datasets)?

Answer: [NA]

Justification: The paper poses no such risks.

Guidelines:

- The answer NA means that the paper poses no such risks.
- Released models that have a high risk for misuse or dual-use should be released with necessary safeguards to allow for controlled use of the model, for example by requiring that users adhere to usage guidelines or restrictions to access the model or implementing safety filters.
- Datasets that have been scraped from the Internet could pose safety risks. The authors should describe how they avoided releasing unsafe images.
- We recognize that providing effective safeguards is challenging, and many papers do not require this, but we encourage authors to take this into account and make a best faith effort.

## 12. Licenses for existing assets

Question: Are the creators or original owners of assets (e.g., code, data, models), used in the paper, properly credited and are the license and terms of use explicitly mentioned and properly respected?

Answer: [Yes]

Justification: The data and code used in this paper have obtained legal permissions.

Guidelines:

- The answer NA means that the paper does not use existing assets.
- The authors should cite the original paper that produced the code package or dataset.
- The authors should state which version of the asset is used and, if possible, include a URL.
- The name of the license (e.g., CC-BY 4.0) should be included for each asset.

- For scraped data from a particular source (e.g., website), the copyright and terms of service of that source should be provided.
- If assets are released, the license, copyright information, and terms of use in the package should be provided. For popular datasets, [paperswithcode.com/datasets](http://paperswithcode.com/datasets) has curated licenses for some datasets. Their licensing guide can help determine the license of a dataset.
- For existing datasets that are re-packaged, both the original license and the license of the derived asset (if it has changed) should be provided.
- If this information is not available online, the authors are encouraged to reach out to the asset's creators.

### 13. New Assets

Question: Are new assets introduced in the paper well documented and is the documentation provided alongside the assets?

Answer: [NA]

Justification: The paper does not release new assets.

Guidelines:

- The answer NA means that the paper does not release new assets.
- Researchers should communicate the details of the dataset/code/model as part of their submissions via structured templates. This includes details about training, license, limitations, etc.
- The paper should discuss whether and how consent was obtained from people whose asset is used.
- At submission time, remember to anonymize your assets (if applicable). You can either create an anonymized URL or include an anonymized zip file.

### 14. Crowdsourcing and Research with Human Subjects

Question: For crowdsourcing experiments and research with human subjects, does the paper include the full text of instructions given to participants and screenshots, if applicable, as well as details about compensation (if any)?

Answer: [NA]

Justification: The paper does not involve crowdsourcing nor research with human subjects.

Guidelines:

- The answer NA means that the paper does not involve crowdsourcing nor research with human subjects.
- Including this information in the supplemental material is fine, but if the main contribution of the paper involves human subjects, then as much detail as possible should be included in the main paper.
- According to the NeurIPS Code of Ethics, workers involved in data collection, curation, or other labor should be paid at least the minimum wage in the country of the data collector.

### 15. Institutional Review Board (IRB) Approvals or Equivalent for Research with Human Subjects

Question: Does the paper describe potential risks incurred by study participants, whether such risks were disclosed to the subjects, and whether Institutional Review Board (IRB) approvals (or an equivalent approval/review based on the requirements of your country or institution) were obtained?

Answer: [NA]

Justification: The paper does not involve crowdsourcing nor research with human subjects.

Guidelines:

- The answer NA means that the paper does not involve crowdsourcing nor research with human subjects.

- Depending on the country in which research is conducted, IRB approval (or equivalent) may be required for any human subjects research. If you obtained IRB approval, you should clearly state this in the paper.
- We recognize that the procedures for this may vary significantly between institutions and locations, and we expect authors to adhere to the NeurIPS Code of Ethics and the guidelines for their institution.
- For initial submissions, do not include any information that would break anonymity (if applicable), such as the institution conducting the review.